UNITED NATIONS UNIVERSITY
GEOTHERMAL TRAINING PROGRAMME
Orkustofnun, Grensasvegur 9,
IS-108 Reykjavik, Iceland

Reports 2011
Number 8

RESISTIVITY IMAGING OF THE SANTA MARIA SECTOR AND THE NORTHERN ZONE OF LAS PAILAS GEOTHERMAL AREA, COSTA RICA, USING JOINT 1D INVERSION OF TDEM AND MT DATA

Diego Badilla Elizondo
Instituto Costarricense de Electricidad (ICE)
P.O. Box 10032
Sabana Norte, San José
COSTA RICA
dbadillae@ice.go.cr

ABSTRACT

In this geophysical research work, data from MT and TDEM surveys are processed, inverted and discussed to explain the electrical resistivity of the subsurface of two specific areas located north and east of Las Pailas geothermal field in Costa Rica. The static shift problem of MT data is solved by inverting jointly both TDEM and MT data. Seven profiles are analysed, based on 1D models from 22 MT and 19 TDEM soundings. Resistivity cross-sections and iso-resistivity maps were compiled from the 1D models of the inverted TDEM and MT data. The main idea was to analyse the subsurface resistivity structure of those areas and also to compare the results with a discontinuity known as NF7, trying to see if the existing MT and TDEM data could reveal a more detailed model of the zone that can be of use in future expansion of the production field. The main result of the survey is the probable confirmation of the NF7 structure on the northern side of the survey area and in the Santa María sector. Another important fact was the appearance of a low-resistivity body (deep conductor) in the northern part of the study area and in the Santa María sector, interpreted as a possible heat source.

1. INTRODUCTION

Geophysical exploration for geothermal resources has become an essential tool that, together with geochemistry and geology, plays a very important role in the exploration campaign of a geothermal area. Resistivity is directly related to the properties of interest, like salinity, temperature, porosity (permeability) and alteration. To a great extent, these parameters characterize the reservoir (Hersir and Björnsson, 1991). This capacity of the resistivity makes resistivity measurements the most powerful geophysical method in geothermal exploration.

Las Pailas geothermal area is located on the southern part of the Rincón de la Vieja Volcano. The Rincón de la Vieja volcano belongs to the Guanacaste volcanic range, and is located between the Miravalles and Orosí volcanoes. Las Pailas geothermal field is now producing 35 MW of electricity, but the idea is to increase the production of the field in a few years.

The objective of this work was to obtain more details on the subsurface resistivity structure to the north and east of Las Pailas geothermal field, especially in the zone of Santa Maria which is located 3 km to the east and north of well 2. The work was done using data collected with two of the most important electromagnetic methods: the magnetotelluric (MT) and the time domain electromagnetic (TDEM), applying Phoenix Geophysics equipment MTU-5A and V8. Data were collected by the personnel from the Geophysics Department of the Costa Rican Electricity Company (ICE) in collaboration with the Geothermal Resources Service Centre (CSRG). These data were processed, edited and finally modelled to produce different presentations such as maps and cross-sections revealing the subsurface resistivity structure of the area.

For the Geothermal Resources Service Centre (CSRG), the main division of the Costa Rican Electricity Company (ICE) in charge of exploration, development and exploitation of the geothermal resources, this survey becomes very important because the area under study is a part of the Las Pailas geothermal field, and the results could help to decide if the zone is profitable for future extension of the production field.

The survey was done on profiles mainly across one important discontinuity of the zone, known as NF7, according to the existing MT and TDEM data. This structure was suggested in the geothermal model proposed by the Geothermal Resources Service Center (CSRG) Geology Department, and by the consulting company, West Japan Engineering Consultants (WestJEC).

In this specific project, 1D inversion models were used of the rotationally invariant determinant of the apparent resistivity of MT. The main reason for that is because the time allotted to process and analyse the data was not enough to do 2D or 3D inversion.

Preliminary model calculations and reported geothermal industry experience indicate that a smooth, minimum structure 1D inversion of the rotationally invariant determinant data of MT can reproduce complex 3D resistivity structures, while 1D inversion of either xy or yx modes can give misleading results (Árnason, et al., 2010).

2. RESISTIVITY OF ROCKS

2.1 Specific resistivity

The specific resistivity, ρ, is an electrical characteristic that depends on the material and it is measured in Ohm-meters (Ωm). The reciprocal of resistivity is called conductivity, σ, measured in Siemens/m (S/m). Resistivity can be defined for a piece of a specific material as the ratio of the potential difference, ΔV (V) to the current, I (A), across the material which has a cross-sectional area A and length L (Figure 1):

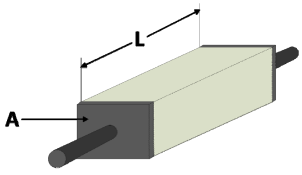

FIGURE 1: Material with length L and cross-sectional area A

$$\rho = \frac{\Delta V}{I}\frac{A}{L} = R\frac{A}{L} \tag{1}$$

where ρ = Specific resistivity of the material (Ωm);
R = Electrical resistance of the material (Ω);
L = Length (m);
A = Cross-sectional area of the conducting material (m^2).

The specific resistivity can also be related to the electrical field through Ohm´s Law. The electrical field strength, $\boldsymbol{E}$ (V/m) at a point in a material is proportional to the current density, $\boldsymbol{j}$ (A/m^2):

$$\boldsymbol{E} = \rho \boldsymbol{j} \tag{2}$$

In this equation, ρ, acts like a proportional constant because it depends on the material, as mentioned above.

Electrical conductivity in minerals and solutions takes place by the movement of electrons and ions. Most rocks near the earth's surface have low conductivity. Conduction of electricity is mostly through groundwater contained in pores of the rocks and along surface layers at the contact of rocks and solution (Hersir and Árnason, 2009).

2.2 Factors affecting electrical resistivity of water-bearing rocks

In geothermal areas the rocks are water-saturated. The ionic conduction in this condition depends on the number and mobility of ions and on the rock matrix, because conduction is also defined by the connectivity of the flow paths through the rock.

The resistivity of rocks is affected by various factors. The rock matrix itself is usually an insulator and for the rocks near the earth's surface, electric conduction occurs through an aqueous solution of common salts distributed throughout the pores of the rocks. The main factors that control the resistivity of rocks are:

- Temperature
- Porosity and permeability
- Salinity
- Water-rock interaction and alteration

2.2.1 Temperature

At moderate temperatures, 0-200°C, resistivity of aqueous solutions decreases with increasing temperature as shown in Figure 2 and 3. The reason is increasing mobility of the ions caused by a decrease in the viscosity of the water. The relationship between resistivity and temperature of rock saturated with an electrolyte has been described by Dakhnov (1962) as:

$$\rho_w = \frac{\rho_{w_o}}{1 + \alpha(T - T_o)} \tag{3}$$

where ρ_w = Resistivity of the fluid at temperature T (Ωm);
ρ_{wo} = Resistivity of the fluid at temperature T_0 (Ωm);
α = Temperature coefficient of resistivity (°C^{-1});
$\alpha \approx 0.023$°C^{-1} for $T_0 = 23$°C, and 0.025°C^{-1} for $T_0 = 0$°C;
T_0 = Reference temperature (°C).

At high temperatures, a decrease in the dielectric permittivity of the water results in a decrease in the number of dissociated ions in the solution. Above 300°C, this starts to increase fluid resistivity (Quist and Marshall, 1968) as seen in Figure 2.

2.2.2 Porosity and permeability

The fractional porosity, ϕ_t, of a material is defined as the ratio of the pore volume to the total volume of the material. There are primarily three types of porosity: inter-granular (pores formed as spaces between grains), joints-fissures (net of fine fractures) and vugular (big and irregular pores formed as a material is dissolved or by gas). Fractional porosity is given by the formula:

$$\phi_t = \frac{V_\varphi}{V} \tag{4}$$

where ϕ_t = Fractional porosity;
V_φ = Volume of voids;
V = Total volume of the material.

It has been observed for many cases that resistivity of water-bearing rocks varies approximately as the inverse square of the porosity. This empirical law, called Archie's law (Archie, 1942) describes how resistivity depends on porosity if ionic conduction in the pore fluid dominates other conduction mechanisms in the rocks (Hersir and Árnason, 2009):

$$\rho = \rho_w a \phi_t^{-n} \tag{5}$$

where ρ = Bulk (measured) resistivity (Ωm);
ρ_w = Resistivity of the pore fluid (Ωm);
a = An empirical parameter, usually around 1;
ϕ_t = Porosity in proportions of total volume;
n = Cementing factor, an empirical parameter which varies from 1.2 for unconsolidated sediments to 3.5 for crystalline rocks, usually around 2

It is known that Equation 5 can be expressed as:

$$\rho = \rho_w F \tag{6}$$

where F represents a factor called the formation factor: $F = a\phi_t^{-n}$.

Permeability represents a measure of how fluids flow through a porous solid. A rock may be highly porous, but if the pores are isolated, it will have no permeability and the rock may not conduct electricity. Here is when the concept of effective porosity is important, because effective porosity represents the degree to which pores within the solid are interconnected. Usually, permeability is directional in nature, but secondary porosity like fractures frequently have a significant impact on the permeability of the material. In addition to the characteristics of the host material, the viscosity and pressure of the fluid also affect the rate at which the fluid will flow (Lee et al., 2003).

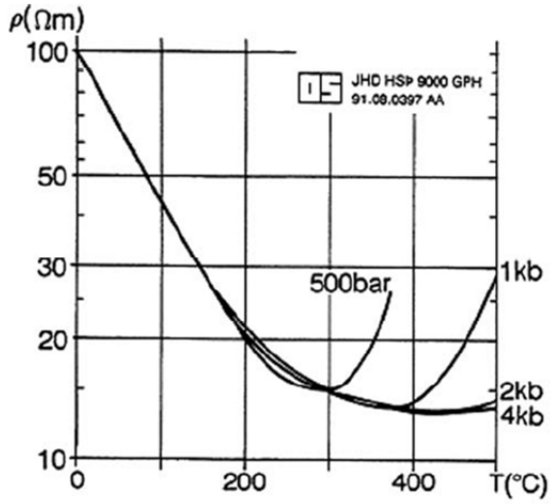

FIGURE 2: Electrical resistivity of a NaCl solution as a function of temperature at different pressures (taken from Hersir and Björnsson, 1991; modified from Quist and Marshall, 1968)

2.2.3 Salinity

It is known that groundwater may have a variety of salts in the solution and that it is not easy to compute resistivity of water from a chemical analysis. The bulk resistivity of a rock is mainly controlled by the resistivity of the pore fluid which is dependent on the salinity of the fluid. An increase in the amount of dissolved solids in the pore fluid can increase the conductivity by large amounts (Figure 3). Conduction in solutions is largely a function of salinity and mobility of the ions present in the solution. The conductivity (σ) of a solution depends on the mobility and concentration of the ions present in the solution. This relationship is described by the following equation (Keller and Frischknecht, 1966):

$$\sigma = \frac{1}{\rho} = F(c_1 q_1 m_1 + c_2 q_2 m_2 + \cdots) \quad (7)$$

where σ = Conductivity (S/m);
F = Faraday's number (9.65×10^4 C);
c_i = Concentration of ions;
q_i = Valence of ions;
m_i = Mobility of ions.

As shown in Figure 3, when the amount of dissolved ions in the pore fluid increases, conductivity increases, so it is clearly seen that salinity of electrolytes in water affects conductivity in a nearly inversely linear manner.

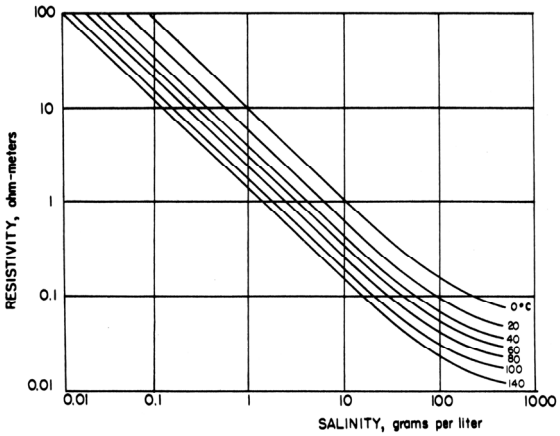

FIGURE 3: The resistivity of solutions of sodium chloride as a function of concentration and temperature (from Keller and Frischknecht, 1966)

2.2.4 Water-rock interaction and alteration

Alteration processes and the resulting type of alteration minerals are dependent on the type of primary minerals, the chemical composition of the geothermal fluid and temperature. The intensity of the alteration is furthermore dependent on temperature, time and the texture of the host rocks.

In Figure 4, the general resistivity structure of high-temperature fields in Iceland is shown. As we can see, alteration intensity is normally low for temperatures below 50-100°C. At those depths the resistivity is relatively high and the conduction is mainly pore fluid conduction. Then alteration increases and the resistivity decreases as the smectite zeolite alteration zone is reached. Smectite naturally occurring due to weathering, diagenesis and hydrothermal alteration, is considered to be formed at low pressure and at temperatures less than about 200°C (Pytte and Reynolds, 1989; Tucker, 1991). In this alteration zone, mineral conduction becomes the dominant conduction mechanism; this is because the inter-layer cations of smectites are mostly exchangeable, but it has been noted that the cation exchange capacity is sometimes in excess. The principal cause of cation exchange is the unbalance of charge in the fundamental layers, but some additional exchange could take place through unsatisfied surface valences. The inter layer spaces in smectites can be penetrated not only by water and exchange cations but also by certain organic cations and by various organic liquids. On heating, the inter-layer water of smectites is lost, mostly between 100 and 250°C, but some remains to about 300°C (Deer et al., 1962).

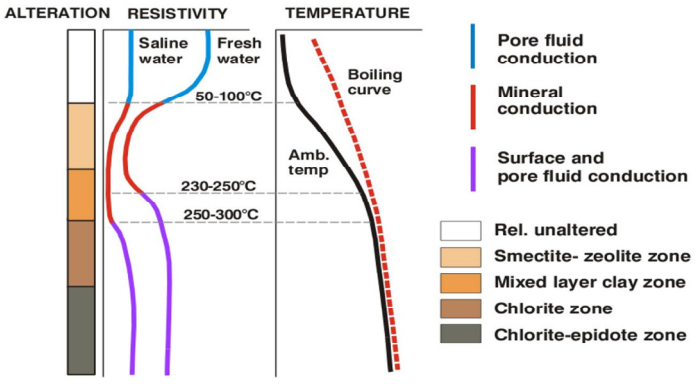

FIGURE 4: A summary of general resistivity structures of high-temperature fields in Iceland (from Flóvenz et al., 2005)

Below the smectite zeolite zone, the mixed clay zone becomes dominant and the resistivity increases again, most likely due to strongly reduced cation exchange capacity of the clay minerals in the mixed clay and chlorite zone. Here, surface and pore fluid conduction probably dominates as the mineral conduction is diminished. The transition from smectite to mixed layer clay happens at a temperature of around 230-250°C, and there we have the high-resistivity core (again due to strongly reduced cation

exchange capacity of the alteration minerals) with temperatures higher than 250°C where alteration minerals like chloride and epidote are present.

Resistivity reflects alteration mineralogy but not necessary temperature (Árnason et al., 2000). If the alteration and temperature are in equilibrium, the resistivity structure reflects not only the alteration but also temperature and, in most cases, it can be regarded as a "maximum thermometer". It means that if the temperature that produced the alteration mineralogy prevails, the resistivity structure can be used to predict the temperature but, if cooling occurs, the alteration remains and so does the resistivity structure. However, there have been occurrences where alteration minerals have indicated a lower temperature than that measured in the wells. This has been interpreted as being due to a young system being heated up and the alteration is lagging behind, still not in equilibrium with the temperature (Hersir and Árnason, 2009).

The relationship between temperature and alteration can also be appreciated in Figure 5. The smectite and the zeolites minerals have loosely bound cations that make these minerals conductive, while in the chlorite mineral these ions are bound in a crystal lattice (Deer et al., 1962) which makes the mineral more resistive. A similar correlation has been found in all the explored and drilled high-temperature geothermal fields in Iceland as well as in many high-temperature areas in other countries where the host rocks are volcanic (Árnason et al., 2010).

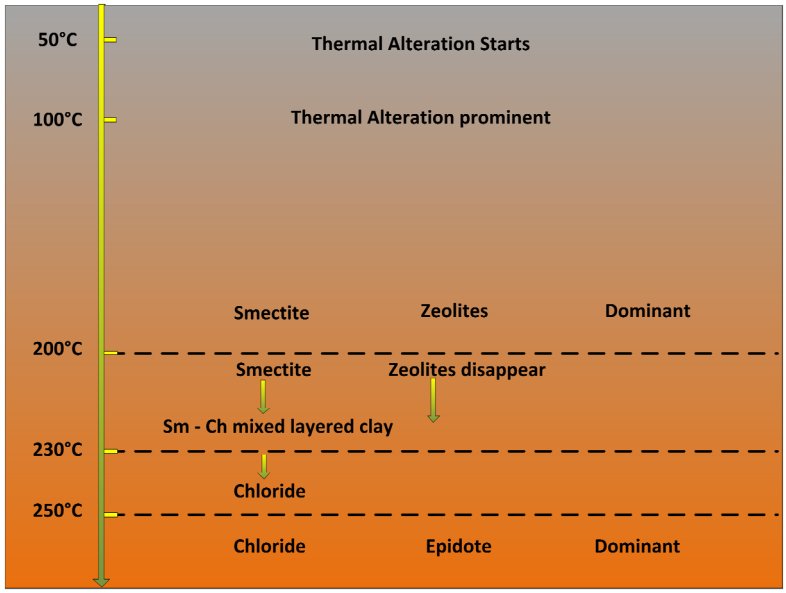

FIGURE 5: Alteration mineralogy and temperature (modified from Hersir and Árnason, 2009)

3. TDEM METHOD

3.1 Central loop transient electromagnetic method

In the central-loop TDEM sounding method, the current in the ground is generated by a time-varying field of a controlled magnitude generated by a source loop. A loop of wire is placed on the ground and a constant magnetic field of known strength is built up by transmitting a constant current into the loop (Figure 6).

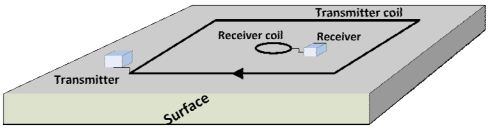

FIGURE 6: Typical central loop TDEM configuration (modified from Rowland, 2002)

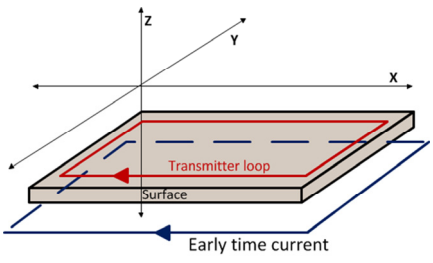

FIGURE 7: Current propagation, early time (modified from Rowland, 2002)

Just a few milliseconds after the constant current is injected into the loop, it is abruptly turned off. The resultant decaying magnetic field induces electrical currents in the ground; these induced currents are initially concentrated below the transmitter loop, called the early time (Figure 7), but then the

current diffuses downwards and away from the transmitter, and that is called the late time (Figure 8).

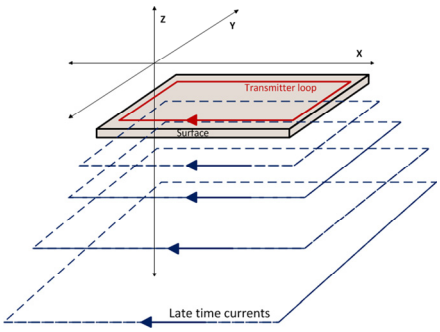

FIGURE 8: Current propagation, late time (modified from Rowland, 2002)

If the current is turned off instantaneously, it would induce infinite voltage in the source loop. Practically, the current is not abruptly turned off but rather in a linear manner in an interval of time called turn-off time (TOFF). The turn-off time is measured by the transmitter and fed by the operator into the receiver (Árnason, 2006a).

With this process, the current distribution in the ground generates a secondary magnetic field that decays with time. The decay rate of the secondary magnetic field as a function of time is monitored by measuring the voltage induced in a receiver coil at the centre of the transmitting loop in time gates (Figure 9). The current distribution and the decay rate of the secondary magnetic field depend on the resistivity structure of the earth. The decay rate, recorded as a function of time after the current in the transmitter loop is turned off can, therefore, be interpreted in terms of the subsurface resistivity structure (Árnason, 1989).

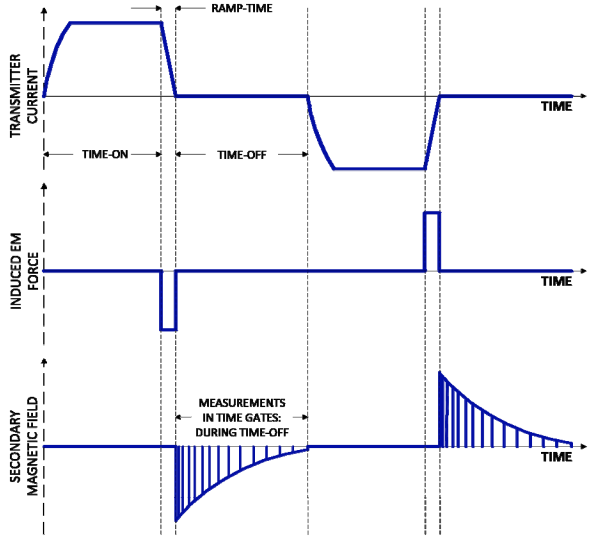

FIGURE 9: TDEM waveforms (modified from Rowland, 2002)

3.2 TDEM response for a homogeneous earth

For a homogeneous half space of conductivity σ, the induced voltage in the receiving coil is given by (Árnason, 1989):

$$V(t,r) = I_0 \frac{C(\mu_0 \sigma r^2)^{\frac{3}{2}}}{10\pi^{\frac{1}{2}} t^{\frac{5}{2}}} \qquad (8)$$

$$\text{where} \quad C = A_r n_r A_s n_s \frac{\mu_0}{2\pi r^3}$$

The time behaviour of the diffusing voltage response for different resistivities has the same character and can be divided in three phases: early times, intermediate times and late times. As we can see in Figure 10, the induced voltage is constant at the early stage and starts to decrease with time in the intermediate stage. At late times, the measured voltage $V(t)$ decays over time in such a way that the logarithm of the induced voltage decreases linearly as a function of the logarithm of time, and in this last stage the slope of the curve is -5/2, showing that the voltage is proportional to $t^{-5/2}$ and varies as $\sigma^{3/2}$ (Árnason, 1989).

In Figure 10 it can also be seen, that the early time response depends on resistivity, because it increases as resistivity increases; also, there is a variation (stages are shifted) in the transition from early time to intermediate and from intermediate to late time depending on the resistivity.

Apparent resistivity, ρ_a, of a homogeneous half-space in terms of induced voltage at late times after the source current is turned off is given by (Árnason, 1989):

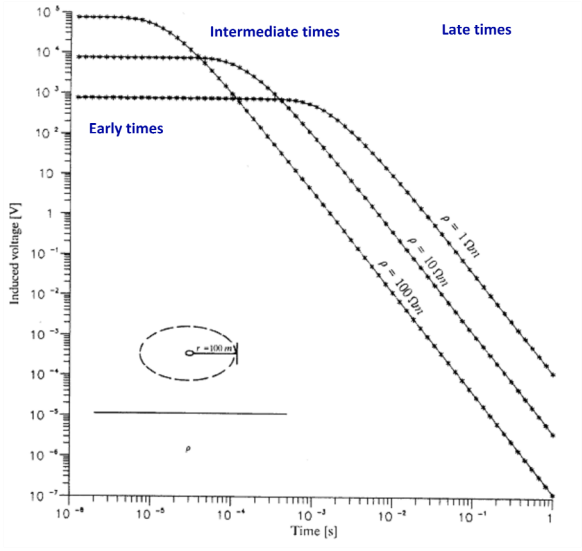

FIGURE 10: Voltage response for a homogeneous half-space (modified from Árnason, 1989)

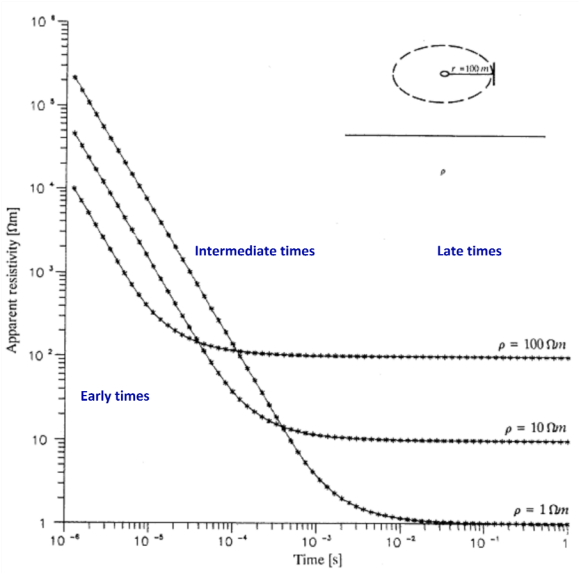

FIGURE 11: Late time apparent resistivity for a homogeneous half-space (modified from Árnason, 1989)

$$\rho_a = \frac{\mu_0}{4\pi}\left[\frac{2\mu_0 A_r n_r A_s n_s I_0}{5t^{\frac{5}{2}}V(t,r)}\right]^{\frac{3}{2}} \tag{9}$$

where t = Elapsed time after the transmitter current is turned off (s);
A_r = Cross-sectional area of the receiver coil (m^2);
n_r = Number of windings in the receiver coil;
μ_0 = Magnetic permeability in vacuum (H/m);
A_s = Cross-sectional area of the transmitter loop (m^2);
n_s = Number of windings in the transmitter loop;
I_0 = Transmitter current (A);
$V(t,r)$ = Measured voltage (V).

Figure 11, shows the behaviour of the apparent resistivity response for different values of the resistivity of a homogeneous half-space. It is possible to see that the apparent resistivity approaches the true resistivity of the half-space at late times as it gets lower values. This is an important fact because we can relate it to the voltage response which reaches the late stage at late times, as the resistivity is lower, shown in Figure 11. Here we can also see how the transition between early time, intermediate and late time depends on the resistivity; it is shifted to early times and higher resistivity values.

4. MT METHOD

4.1 Basic principles

The magnetotelluric (MT) technique is a passive electromagnetic (EM) technique; it means that the measured signals are natural and not artificial like in the TDEM method, which is an active method where an artificial current is transmitted into a loop. MT technique involves measuring fluctuations in the earth's natural electric, **E**, and magnetic, **B**, fields in orthogonal directions (see Figure 12) at the

surface of the earth as a means of determining the conductivity structure of the earth at depths ranging from a few tens of meters down to several hundreds of kilometres (Simpson and Bahr, 2005).

In the fifties, the most fundamental theory of exploration MT was propounded by Tikhonov (1950), but then it was given in more detail by Cagniard (1953). The central idea of this theory was the realisation that electromagnetic responses from any depth could be obtained simply by extending the magnetotelluric sounding period.

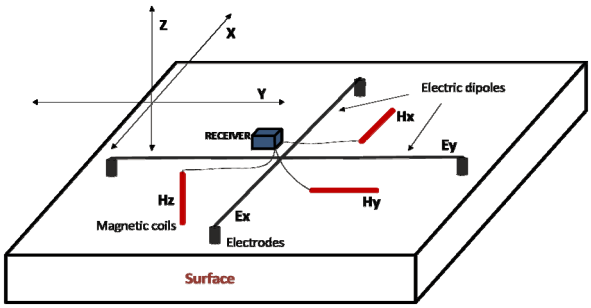

FIGURE 12: MT basic configuration (Phoenix Geophysics, 2009)

Resistivity can be expressed as the ratio of the orthogonal electric, **E**, and magnetic, **B**, fields as a function of the period T, given by Equation 10:

$$\rho = \frac{1}{\omega\mu}\left|\frac{\mathbf{E}}{\mathbf{H}}\right|^2 = 0.2T\left|\frac{\mathbf{E}'}{\mathbf{B}'}\right|^2 \tag{10}$$

where ω = Angular frequency ($2\pi f$);
μ = Magnetic permeability (H/m);
$\mathbf{E}$ = Electric field (V/m);
$\mathbf{H}$ = Magnetic intensity (A/m);
$\mathbf{E}'$ = Electrical field (mV/km);
$\mathbf{B}'$ = Magnetic induction (nT), $\mathbf{B}' = \mu\mathbf{H} \cdot 10^{-9}$;

The principle of MT is based in the *electromagnetic skin depth* relationship, which describes the exponential decay of electromagnetic fields as they diffuse into a medium. At the depth, $\delta(T)$, the electromagnetic field has attenuated to e^{-1} of the amplitudes at the surface of the earth. This exponential decay of electromagnetic fields with increasing depth renders them insensitive to conductivity structures lying deeper than $\delta(T)$. Hence, in MT studies, electromagnetic skin depth is generally equated with the *penetration depth* of electromagnetic fields in the earth (Simpson and Bahr, 2005):

$$\delta(T) = 500\sqrt{T\rho} \tag{11}$$

where δ = Skin depth (m);
ρ = Resistivity, or the average resistivity of an equivalent uniform half-space.

4.2 Assumptions of the MT method

For the purposes of considering electromagnetic induction in the earth, a number of simplifying assumptions are considered applicable (Simpson and Bahr, 2005):

- ✓ Maxwell's general electromagnetic equations are obeyed.
- ✓ The natural electromagnetic source fields utilised, being generated by large-scale ionospheric current systems that are relatively far away from the earth's surface, may be treated as uniform, plane-polarised electromagnetic waves impinging on the earth at near-vertical incidence. This assumption may be violated in polar and equatorial regions.

- ✓ No accumulation of free charges is expected to be sustained within a layered earth. In a multi-dimensional earth, charges can accumulate along discontinuities. This generates a non-inductive phenomenon known as static shift.
- ✓ Charge is conserved, and the earth behaves as an Ohmic conductor, obeying the equation:

$$\mathbf{j} = \sigma\mathbf{E} \tag{12}$$

where **j** = Total electric current density (A/m^2);
σ = Conductivity of the sounding medium (S/m); and
E = The electric field (V/m).

- ✓ The electric displacement field is quasi-static for MT sounding periods. Therefore, time-varying displacement currents (arising from polarisation effects) are negligible compared with time-varying conduction currents, which promotes the treatment of electromagnetic induction in the earth purely as a diffusion process.
- ✓ Any variations in the electrical permittivities and magnetic permeabilities of rocks are assumed negligible compared with variations in bulk rock conductivities.

4.3 Impedance tensor (Z) and dimensionality

The impedance tensor relates the orthogonal components of the horizontal electric and magnetic fields:

$$\begin{pmatrix} E_x \\ E_y \end{pmatrix} = \begin{pmatrix} Z_{xx}\, Z_{xy} \\ Z_{yx}\, Z_{yy} \end{pmatrix} \begin{pmatrix} H_x \\ H_y \end{pmatrix} \ (\mathbf{E} = \mathbf{ZH}) \tag{13}$$

or

$$E_x = Z_{xx}H_x + Z_{xy}H_y \tag{14}$$

$$E_y = Z_{yx}H_x + Z_{yy}H_y \tag{15}$$

Each component of the impedance tensor, Z_{ij}, is composed of real and imaginary parts. They have both magnitude and phase:

$$\rho_{a\,ij} = \frac{1}{\mu_0 \omega} \left| Z_{ij}(\omega) \right|^2 \tag{16}$$

$$\emptyset_{\,ij} = tan^{-1}\left(\frac{Im\{Z_{ij}\}}{Re\{Z_{ij}\}}\right) \tag{17}$$

For a 1D earth, conductivity varies only with depth and consequently the diagonal elements of the impedance tensors, Z_{xx} and Z_{yy} (which couple parallel electric and magnetic field components) are zero, while the off-diagonal components (which couple orthogonal electric and magnetic field components) are equal in magnitude, but have opposite signs:

$$\left.\begin{aligned} Z_{xx} &= Z_{yy} = 0 \\ Z_{xy} &= -Z_{yx} \end{aligned}\right\} 1-D \tag{18}$$

For homogeneous earth (1D), when electromagnetic plane waves propagate vertically downward, the ratio of the electric to the magnetic field intensity is a characteristic measurement of the electromagnetic properties of the medium (Keller and Frischknecht, 1966):

$$Z_{xy} = \frac{i\omega\mu_0}{k} = \frac{E_x}{H_y} = -\frac{E_y}{H_x} \tag{19}$$

where Z_{xy} = Characteristic impedance;
ω = Angular frequency ($2\pi f$), where f is frequency (Hz);
μ_0 = Magnetic permeability in vacuum (H/m);
$E_{x,y}$ = Electric field (V/m) in *x, y* direction;
$H_{x,y}$ = Magnetic intensity (A/m) in *x, y* direction;
k = $\sqrt{i\omega\mu_o(i\omega\varepsilon + \sigma)}$ is the wave propagation number;
ε = Dielectric permittivity (F/m);
σ = Electrical conductivity (S/m).

For the quasi-stationary approximation, $\sigma \gg \omega\varepsilon$, the wave propagation number is approximated to $k = \sqrt{i\omega\mu_0\sigma}$ and Equation 19 can be written as:

$$Z_{xy} = \frac{i\omega\mu_0}{\sqrt{i\omega\mu_0\sigma}} = \sqrt{i}\sqrt{\omega\mu_0\rho} = \sqrt{\omega\mu_0\rho}\cdot e^{\frac{i\pi}{4}} \tag{20}$$

Equation 20 shows, in a very clear way, that the phase difference between E_x and H_y is $\pi/4 = 45°$. For homogeneous earth (1D), the resistivity is given as:

$$\rho_{xy} = \frac{1}{\omega\mu_0}\left|Z_{xy}\right|^2;\ \theta_{xy} = \arg(Z_{xy}) \tag{21}$$

$$\rho_{yx} = \frac{1}{\omega\mu_0}\left|Z_{yx}\right|^2;\ \theta_{yx} = \arg(Z_{yx}) \tag{22}$$

Specifically speaking, the apparent resistivity calculated from off-diagonal elements of the impedance tensor for the 1D case like in Equations 21 and 22 should be the same. But, in reality, the earth is never quite 1D, and the two resistivities in the *xy* direction and in the *yx* direction are different. By rotating the impedance tensor, we will obtain different values for the resistivity. This is a serious problem because we don't know which value to use, *x*y or *yx*, as they will give different models.

The method used in this work for 1D inversion was to use the determinant of the impedance tensor, which is rotationally invariant (the resistivity value doesn't change with rotation); it is a kind of an average value of the apparent resistivity (see Figure 16). The determinant value is calculated as shown in Equation 23 and used in the 1D inversion in this report:

$$\rho_{det} = \frac{1}{\omega\mu_o}|Z_{det}|^2 = \frac{1}{\omega\mu_o}\left|\sqrt{Z_{xx}Z_{yy} - Z_{xy}Z_{yx}}\right|^2;\ \theta_{det} = \arg(Z_{det}) \tag{23}$$

In a 2D earth, it is assumed that the resistivity can vary with depth and also in one lateral direction, and that the resistivity is constant in the other horizontal direction. The direction along which the resistivity is constant is called the electric strike. If the field setup coordinate system is not parallel and perpendicular to the electrical strike, the MT impedance tensor data are mathematically rotated with one axis perpendicular to the electrical strike and the other axis parallel to it, through minimizing the off diagonal elements of the impedance tensor. Thereby, we get Z_{xx} and Z_{yy} again equal to zero, like in the 1D case, but the difference is that, in 2D, $Z_{xy} \neq -Z_{yx}$. Sometimes it is not possible to find a strike direction that satisfies the condition: $Z_{xx} = Z_{yy} = 0$, and that is because of the 3D subsurface resistivity structure.

In the 2D case, the magnetotelluric field splits into two independent modes: (1) the TM-mode (transverse magnetic mode – the magnetic field is parallel to the electrical strike direction, transverse to the resistivity structure), and (2) the TE-mode (transverse electric mode – the electric field is parallel to the electrical strike direction, transverse to the resistivity structure). The TM- and TE-modes are frequently referred to as the H-polarization (the magnetic field is polarized along the model strike) and the E-polarization (the electric field is polarized along the model strike).

In the 3D case, conductivity varies in all three directions, x, y and z, and we have $Z_{xy} \neq Z_{yx}$ and $Z_{xx} \neq Z_{yy}$. There is no rotational direction through which the two diagonal components of the impedance tensor become zero simultaneously.

4.3.1 Swift skew

This is a normalized parameter, a rotational invariant, to characterize the geo-electric asymmetry of a medium. It can be expressed as:

$$Skew = S = \frac{|Z_{xx} + Z_{yy}|}{|Z_{xy} - Z_{yx}|} \tag{24}$$

If the value of S is large, it means that we are dealing with a 3D earth, but if we get a small value (for example 0.2), it means that we are working in a 1D or 2D earth. In panel 4 in Figure 16 we can see the black dotted curve which represents the skew and it has values lower than 0.2 for periods lower than 10 s, and that means that probably the resistivity structure at depth, corresponding to that period range below that sounding, is 1D or 2D.

4.4 Layered earth

For horizontally N-layered earth, the plane wave impedance is given by the recursive formula (Ward and Wannamaker, 1983) as:

$$\hat{Z}_N = \frac{\omega\mu_0}{k_N};\ \hat{Z}_{n-1} = Z_{n-1}\frac{\hat{Z}_n + Z_{n-1}\tanh(ik_{n-1}h_{n-1})}{Z_{n-1} + \hat{Z}_n tanh\ (ik_{n-1}h_{n-1})} \tag{25}$$

where Z_n = $\frac{\omega\mu_0}{k_N}$ (intrinsic impedance of the nth layer);
k = $\sqrt{-(i\omega\mu_0\sigma_n)}$;
h_n = Thickness of the nth layer;
$\hat{Z}_n$ = Impedance of the nth layer;
Z_1 = Z_0 = which is the impedance at the surface.

For a two layered earth where the first layer has a resistivity, ρ_1, and the second layer has resistivity, ρ_2, Equation 25 becomes:

$$\hat{Z}_1 = Z_1\frac{\hat{Z}_2 + Z_1\tanh(ik_1h_1)}{Z_1 + \hat{Z}_2\ tanh\ (ik_1h_1)} \tag{26}$$

where $Z_1 = Z_0$ = The impedance at the surface; and

k = $\sqrt{\frac{-i\omega\mu_0}{\rho_1}} = \sqrt{\frac{-i2\pi\mu_0}{\rho_1 T}}$.

4.5 Static shift problem

The MT and DC methods, which are based on measuring the electric field, **E**, on the surface, suffer the static shift problem. Static shift can be caused by any multi-dimensional conductivity contrasts (superficial in-homogeneities) having depths and dimensions less than the true penetration depth of electromagnetic fields. The shift is called "static" because the conservation of current at conductivity discontinuities is not a time-dependent process like, for example, induction. Therefore, the phenomenon of static shift does not affect the phase of the transfer function (Simpson and Bahr, 2005).

There are two mains reasons for MT static shift, aside from topographic distortion:

- *Electric field distortion:* In this case due to the vertical resistivity discontinuity, the electric field (voltage difference over a given length) is lower in the low-resistivity domain. Conductivity discontinuities like the ones shown in Figure 13 cause local distortion of the amplitudes of electric fields as a result of conservation of electric charge, hence causing impedance magnitudes to be enhanced or diminished by real scaling factors.

- *Current distortion (current channelling/ repelling):* Superficial bodies can severely and arbitrarily distort magnetotelluric apparent resistivity data. This will distort the electric field and cause the impedance magnitude to increase or decrease by a real scaling factor and therefore shift the apparent resistivity curve up or down on the log scale. For example, in Figure 14 the superficial body with resistivity, ρ_2 is channelling the current because its resistivity is lower than the rest of the subsurface with resistivity, ρ_2. But if this body would have a resistivity higher than, ρ_1, the current would be repelled by this body.

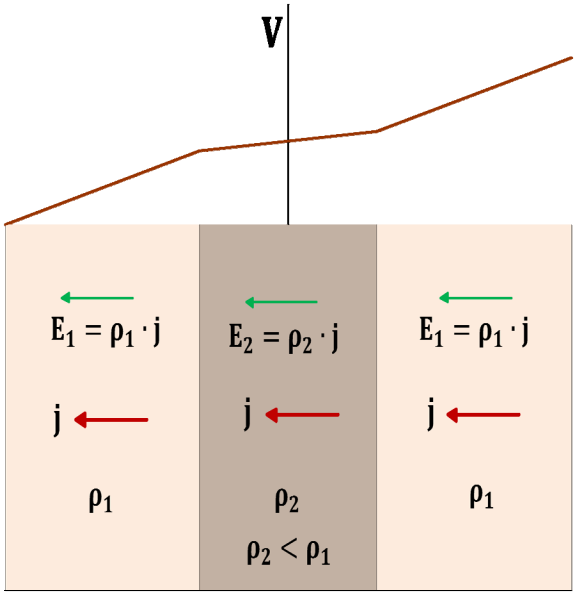

FIGURE 13: Electric field distortion (Sternberg et al., 1988; Árnason, 2008)

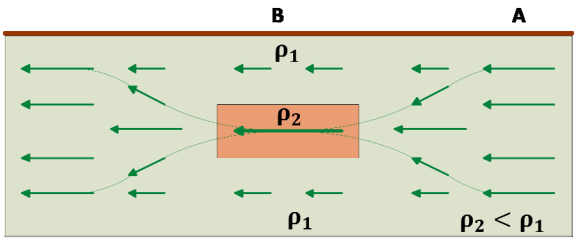

FIGURE 14: Current distortion (Sternberg et al., 1988; Árnason, 2008)

5. DATA PROCESSING AND INVERSION OF TDEM AND MT DATA

5.1 Data processing

TDEM: To prepare the measured data for inversion, the first thing to do was to edit the data; for this a Unix based program called TemX written by Knútur Árnason (2006a) was used. It was specially created to manage files generated by the V8 from Phoenix Geophysics. It performed stacking of the measured values and outliers were thrown out. Finally the .inv file was created, later to be inverted. An example of the inversion result is given in Figure 15. The processed data for all TEM soundings is given in Appendix I (Badilla, 2011).

MT: We used .edi files, the result of processing the data with software from Phoenix, like SSMT2000 and MTEditor. The .edi files were later transformed into Unix files to be used later as an input to

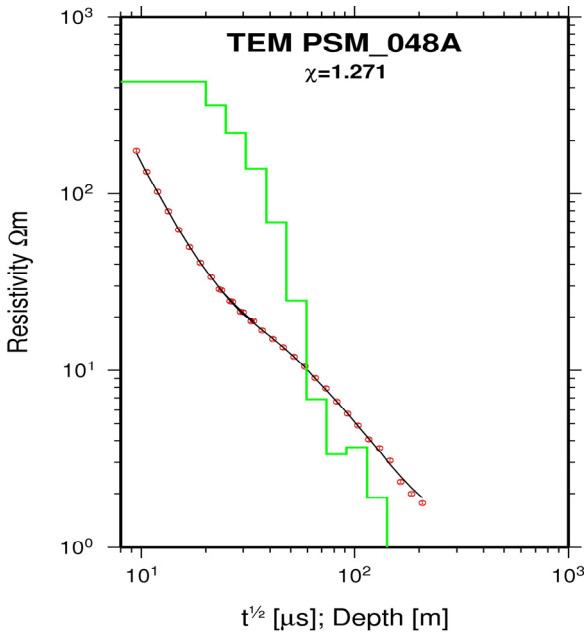

FIGURE 15: TDEM inversion

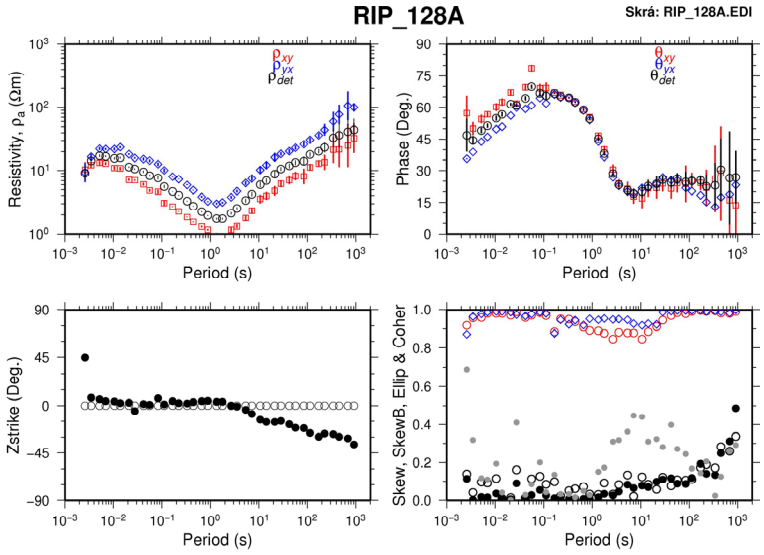

FIGURE 16: Apparent resistivity, phase, Zstrike, skew and coherency calculated in the measured directions, i.e. *x* is magnetic north and *y* magnetic east

ISOR's software. For this purpose some scripts were used like dos2unix, spec2edi and finally edi2ps to generate a graphic file like the one shown in Figure 16. The processed data for all the MT soundings are given in Appendix II (Badilla, 2011).

In the first panel of Figure 16 there are 3 resistivity curves; the red squares represent the measured resistivity in the *xy* direction, the blue diamonds in the *yx* direction and the black circles denote the apparent resistivity derived from the rotationally invariant determinant of impedance tensor, as given in Equation 23. Here it can easily be seen that the resistivity in the *xy* direction is different than in the yx direction, and it means that the earth is not really 1D; but it can also be seen how the determinant values behave very well as an average of those resistivities, and that is why this was used for the 1D inversion of this work. In the second panel (to the right) it is possible to see the phase of the impedance, also in two directions like for the resistivity (red squares and blue diamonds), while black circles denote the apparent phase derived from the rotationally invariant determinant of the impedance tensor. In panel 3, we have the electrical strike (Zstrike) of the impedance, which usually agrees with the geological strike of the area, and it is possible to see how for periods lower than 10 s it is more or less close to zero (Zstrike equals magnetic north), but for periods higher than 10 s it starts to decrease until it reaches the value of -45° at around 1000 s. The fourth panel mainly shows the behaviour of the skew (which is used to characterize the geo-electric asymmetry of a medium) and the coherency, which is a good parameter for analysing the quality of the data; if there is a coherency with values close to 1, it means that our data are well correlated and good.

5.2 Inversion of the data

Data from electromagnetic soundings can be modelled in different ways. We can create a 1D, 2D or even a 3D model of the study area. The difference between the different models is the complexity of the results; also, a more complex and complete model like 3D would take much more time to be developed than a 1D or 2D models. In this report, 1D inversion models of the rotationally invariant determinant of the apparent resistivity were used (see first panel of Figure 16). The main reason for

that is because the time allotted to process and analyse the data was not enough to go through 2D or 3D inversion.

In the beginning of the inversion process only the measured data are available and an initial model as illustrated in Figure 17. The initial model is tested to see how well its response fits with the measured data. Through this initial comparison, it can be evaluated if the fit is good enough. If so that is our final model. However, usually that is not the case and it is necessary to invert the model through the inversion algorithm, which means adjusting the parameters, resistivity and depth for a previously selected number of layers. After that, the inverted model is tested again in the forward algorithm and compared as many times as necessary, in an iteration process, which will improve our model, iteration by iteration, until it is decided that there is a good fit and, with that, the final model.

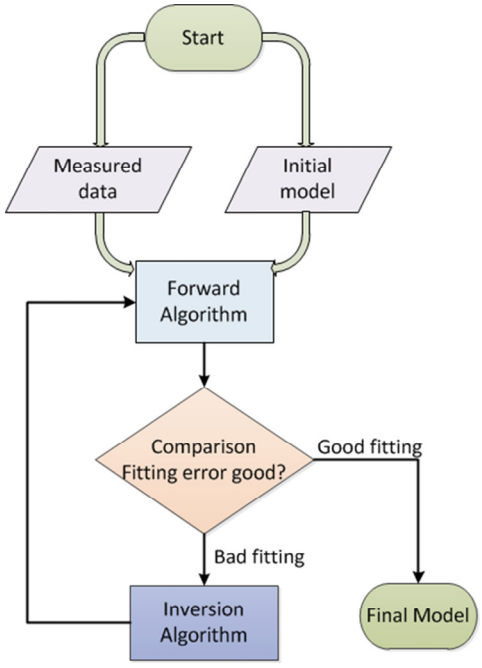

FIGURE 17: The inversion process

The most widely used inversion method, at least for inversion of geo-electric soundings, is the least-square inversion method. In the case where the response depends non-linearly on the model parameters, this method is referred to as a non-linear least-square inversion (Árnason, 1989).

5.3 TDEM inversion

The inversion of the data is done because we are measuring the response of a physical system due to known excitations and we want to determine the relevant physical parameters characterizing the system from the measured response (Árnason, 1989).

A software from ISOR, written by Knútur Árnason (2006b), known as TEMTD, was used to perform the inversion of the TDEM soundings and generate the final resistivity model of the soundings in terms of depth, as shown in Figure 15, where the fit (χ) for the apparent resistivity is shown. The TDEM data and the associated 1D models for all the TDEM soundings are given in Appendix I (Badilla, 2011).The program TEMTD performs 1D inversion with horizontally layered earth models of central-loop Transient Electro-Magnetic (TDEM) data. The program assumes that the source loop is a square loop and that the receiver coil/loop is at the centre of the source loop. The current wave form is assumed to be a half-duty bipolar semi-square wave (equal current-on and current-off segments), with exponential current turn-on and linear current turn-off (Árnason, 2006a).

Once the TDEM inversion models had been made, it was possible to create resistivity cross-sections, but they are not included in this report because they are very shallow and that is not the main purpose of this work.

5.4 Joint 1D inversion of MT and TDEM

In the joint inversion, TDEM soundings are used to correct for the static shift problem of the MT stations. As already discussed, TDEM soundings use only the magnetic field, which is relatively unaffected by the superficial and lateral distortions, to calculate the apparent resistivity below the site.

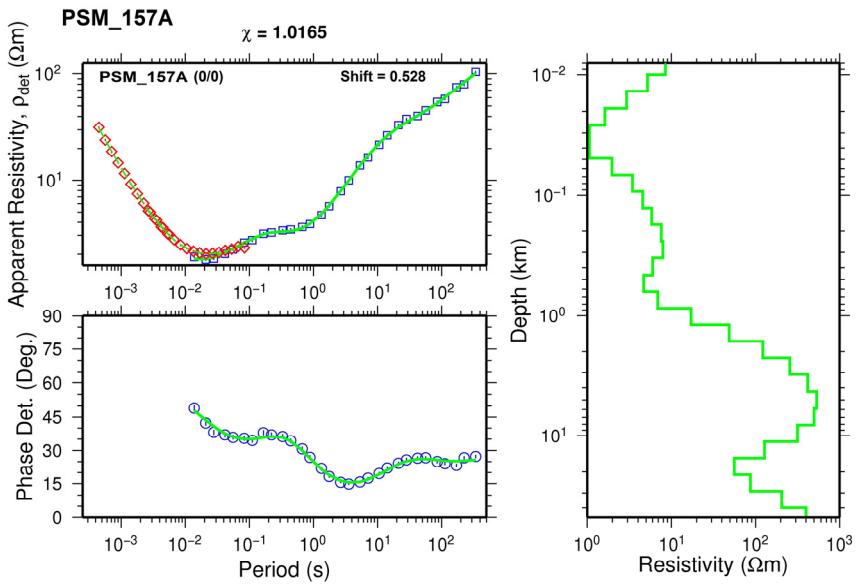

FIGURE 18: Typical result of a joint 1D inversion of TDEM and MT soundings. Red diamonds: TDEM apparent resistivities transformed to a pseudo-MT curve; blue squares: measured apparent resistivities, and blue circles: apparent phase - both derived from the determinant of MT impedance tensor.

The program TEMTD was used again to perform a joint 1D Occam inversion for the rotationally invariant determinant apparent resistivity and phase of the MT soundings and the associated TDEM soundings to obtain the final resistivity model; in this case, it determined the best static shift parameter for the MT data. The 1D models of the joint inversion for all the TDEM and MT data are given in Appendix III (Badilla, 2011).

In the 1D joint inversion, the MT sounding is tied in to the TDEM sounding and the best fitting curve for both the TDEM and the MT data is obtained at the same time as shown in Figure 18. In this figure we have: in the right panel, the resulting 1D resistivity inversion model; in the left panel, its synthetic MT apparent resistivity and phase response. The label on the top of the figure (PSM_157A) is the name of the MT station; the label in the upper left panel (PSM_157A) is the name of the TDEM station. The numbers in parentheses (0/0) indicate that the two stations were 0 m apart and their elevation difference was 0 m. In Figure 18, we can also see the static shift multiplier (0.528).

After getting the results of the joint inversion it was possible to create resistivity cross-sections using the routine TEMCROSS and resistivity maps at different depths using the routine TEMRESD.

6. LAS PAILAS GEOTHERMAL AREA

6.1 Location and tectonic setting of the study area

The most important tectonic feature of the Central American region is the subduction of the Cocos plate under the Caribbean plate along the Middle American trench convergent margin, with rates of nearly 10 cm/year across the Costa Rican segment of the trench (DeMets et al., 1990). That interaction has generated an internal magmatic arc in which the Guanacaste volcanic range comprises the north-western segment (see Figure 19).

Las Pailas geothermal field is located on the southern part of the Rincón de la Vieja volcano. The Rincón de la Vieja volcano belongs to the Guanacaste volcanic range and is located between the Miravalles and Orosí volcanoes. This is characterized as the larger volcanic system of the range.

The last active period occurred in November 1995, generating ash deposits, throwing blocks and tephras, with the development of lahars and mud flows toward the Caribbean coast of Costa Rica (GeothermEx, 2001).

6.2 Geological and structural setting of the study area

The location of Las Pailas geothermal area is clearly related to the activity of a volcano complex, in particular to the Rincón de la Vieja volcano (see Figure 20). It is a composite stratovolcano in the northwest part of Costa Rica, and belongs to the Guanacaste volcanic range, forming a northwest trending ridge consisting of several eruptive centres (Kempter et al., 1996; Kempter, 1997).

The Rincón de la Vieja is a composite, elliptically formed stratovolcano; it comprises an area of approximately 250 km^2, aligned with nine craters in a northwest-southeast direction (Molina, 2000).

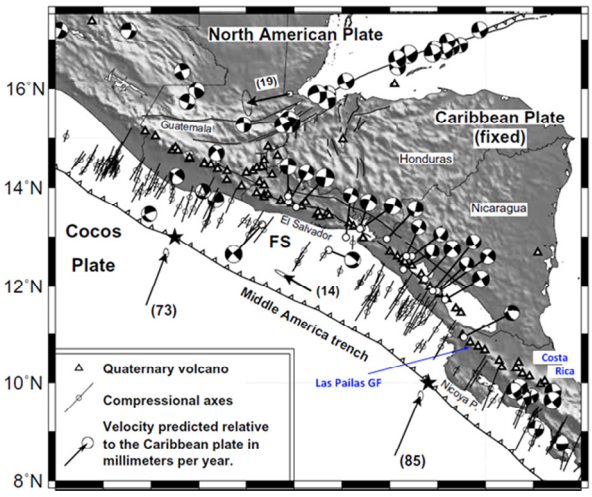

FIGURE 19: Plate tectonics in Central America (modified from DeMets, 2001)

The regional geology of the area includes rocks of the Late Mesozoic-Cenozoic that form the basement and includes sandstones, limestones, conglomerates, volcanic sediments, basalts, associate intrusives and peridotites. Later in the Late Pliocene - Early Pleistocene, rocks of the Aguacate group were deposited. These include lavas from basaltic to dacitic, tuffs, volcanic sediments and ignimbrites. After that, during the Early Pleistocene, thick ignimbrite series of Liberia and Bagaces formations were deposited. Finally, starting in the Late Pleistocene and until the Holocene, the actual Rincón de la Vieja volcano became active. It has erupted mainly materials of basaltic-andesitic composition, which includes lavas, tuffs, pyroclastic flows, ignimbrites and lahars. On the south part of the volcano are four domes of dacitic rhyolitic composition, called Fortuna, San Roque, Góngora and San Vicente, and the Cañas Dulces and Torre hills, of andesitic composition. The ages of these domes and hills vary between 4.3 and 1 m.y. (Molina, 2000; Arias, 2002; Castro, 2002).

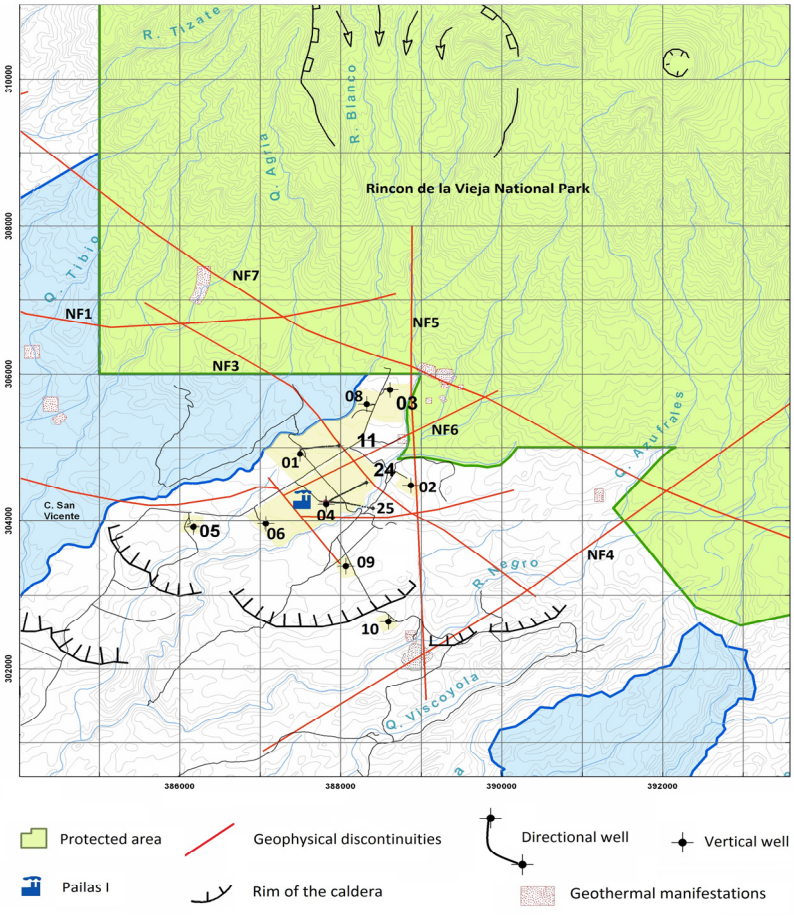

FIGURE 20: Structural setting of Las Pailas geothermal field (taken from ICE internal data and the Department of Geology of the CSRG)

Within Las Pailas geothermal area, inferred faults and lineaments (Figure 20) were defined by a combination of factors including: morphology, field evidence (fractures) of hydrothermal alteration, gravimetric data and resistivity data (Chavarría, et al., 2010).

The structural setting is dominated by normal faults (GeothermEx, 2001); there are also several circular depressions identified that have been interpreted as possible borders of a caldera (GeothermEx, 2001). The main caldera structures are suggested in the area Cañas Dulces and San Vicente. The Cañas Dulces caldera was formed on the southern border by the Cañas Dulces and Torre hills, while the domes San Roque, Góngora and Fortuna are located in the central part of the structure. The San Vicente caldera is clearly defined in the south, while other borders are not defined.

A different structural model for this area was proposed by Arias (2002); the model includes two major strike-slip faults (Cañas Dulces and Las Pailas) with a NW-SE orientation, and probably formed when the Cocos spreading ridge entered the subduction zone. Associated with these faults are several secondary faults with a NE-SW orientation.

6.3 Geothermal manifestations

There are four important superficial geothermal manifestations on the Pacific volcanic side called Las Hornillas, Borinquen, Las Pailas and San Jorge-Santa María (Figure 21), aligned in a NW-SE direction, parallel to the Rincón de la Vieja volcanic axis (Molina, 2000), a good confirmation of structural control for the deep water circulation system in the zone.

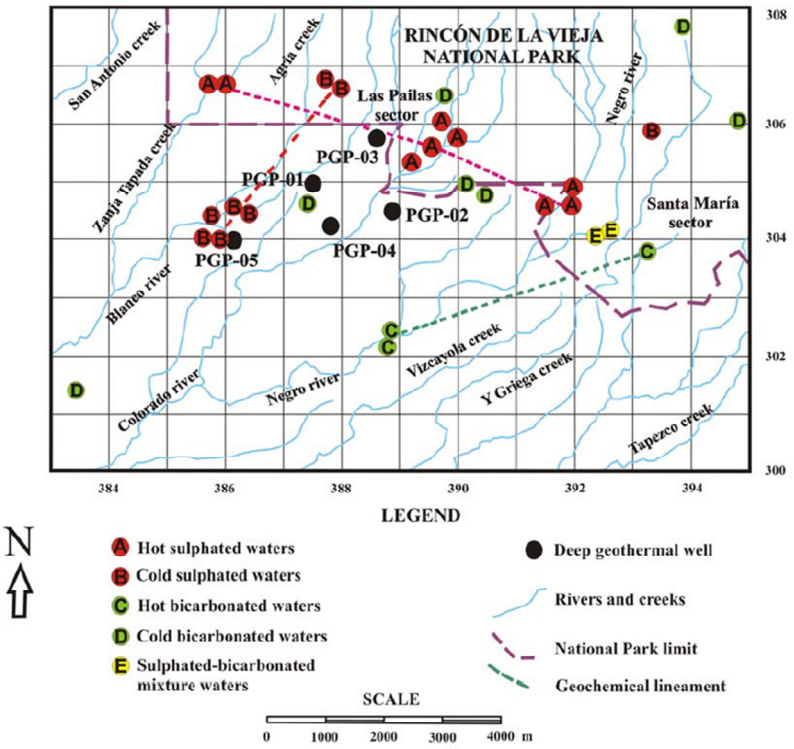

FIGURE 21: Geothermal manifestations in Las Pailas geothermal area (taken from Barrantes, 2006)

Geothermal exploration in the Las Pailas sector has revealed several manifestations. Most of them are inside Rincón de la Vieja national park. With some geochemical studies, thermal and cold springs were characterized, as well as fumaroles with gas and steam emanations (Chavarría et al., 2006).

The hot sulphated waters (A) appear to be related to regional structures with different orientations. They include Las Hornillas, Las Pailas and Santa María manifestations, which are aligned NW-SE and include fumaroles (88-93°C), hot springs (34-96°C) and mud pools (96°C). The cold sulphated waters (B) form a lineament perpendicular (NNE-SSW) to the volcanic axis, with temperatures between 15 and 25°C and are located in the vicinity of the Agria creek and an isolated point in the Santa María sector. Hot bicarbonate waters (C) are located on a NE-SW lineament in the Negro river. They are meteoric waters with geothermal influence, and temperatures between 33 and 56°C. The cold bicarbonate waters (D) are distributed over many places. Their temperatures vary between 16 and

29°C. Finally, sulphated-bicarbonate mixture waters (E) are in the Santa María sector, with temperatures around 40°C, with variable chemical compositions with time; some sulphur deposits have formed (Barrantes, 2006).

6.4 TDEM and MT surveys

Several MT and DC surveys were carried out earlier in Las Pailas geothermal field and in the surroundings, mainly concentrated in the zone of the actual production field and to the northwest. TDEM soundings had not been done in Las Pailas until 2011 because ICE did not have the equipment to carry out those surveys.

Specifically speaking, two small zones in the northeast sector of Las Pailas geothermal area were analysed: the zone known as Santa Maria, which is located 3 km to the east of well 2 (PGP#2), and the zone to the north of well 2, (see Figure 22).

In this work, 22 MT and 19 TDEM soundings were used to create 7 different profiles across the structures known as NF7 and NF4 in Las Pailas geothermal area. The TDEM soundings were collected recently but some of the MT soundings analysed in this work were collected in 2011 and others a few years ago.

These data were chosen because the soundings are located in a very important zone designated for future expansion of the Las Pailas production field where ICE did not have enough data before to create those profiles.

In Figure 22 the location of the study area is shown, the cross-sections, the location of Las Pailas geothermal field, some of the production wells and the boundary of the Rincón de la Vieja National Park. For creating the grid file used in this map and in the other maps and cross-sections, Quantum GIS (1.7.0) was used. It is important to note that the coordinates are in UTM, using the projection wgs84 in zone 16N.

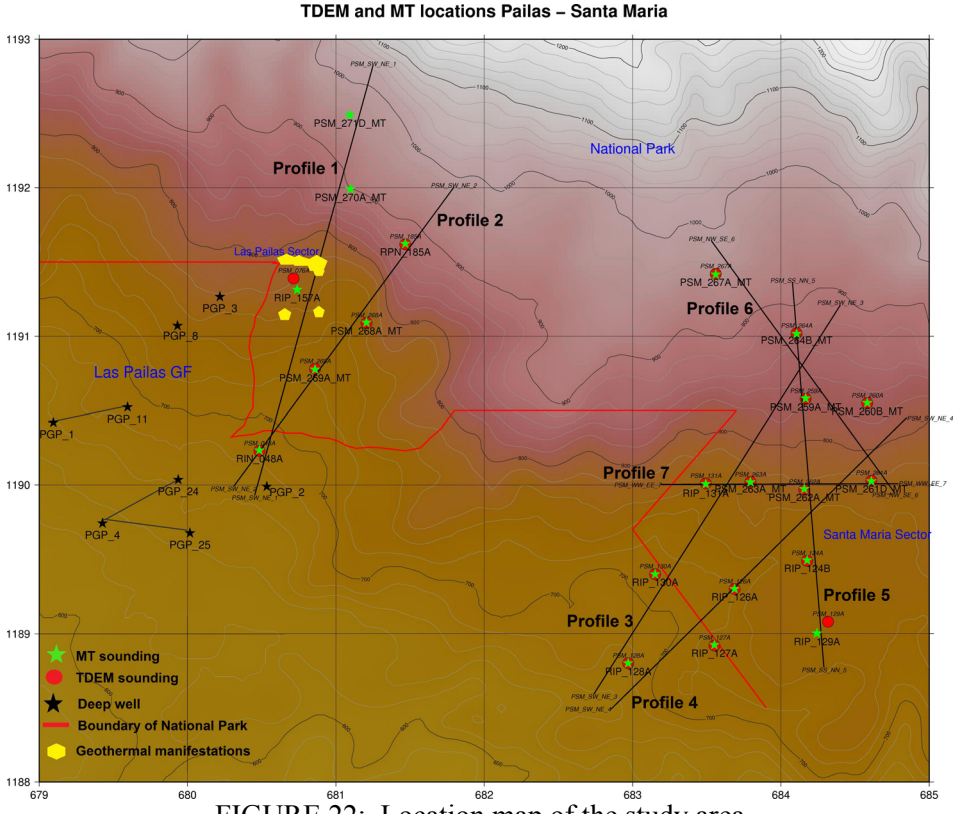

FIGURE 22: Location map of the study area

7. RESULTS OF THE TDEM AND MT SURVEYS

The results given here were obtained through the joint 1D inversion of MT and TDEM data. First, maps of the Zstrike and Tipper strike are shown in two groups: one for high frequency data between 1 and 100 Hz (periods from 1 to 0.01 s) and the other one for low frequency data between 1 and 0.001 Hz (periods from 1 to 1000 s). Then a static shift map and a static shift histogram were created to analyse the behaviour of this parameter in the MT soundings. Finally, the resistivity cross-sections were created using the resulting models for each sounding; in this report cross-sections down to a depth of 5000 and 10000 m b.s.l. are shown, and several iso-resistivity maps were created according to the depth of interest. The maps shown in this work are only valid for the areas where the profiles are located, not for the area between them, because that is only an interpolation effect. All the resistivity cross-sections and iso-resistivity maps are included in a special report with the appendices to this report (Badilla, 2011).

7.1 Electrical strike direction

The electrical strike direction is shown in Figures 23 and 24 for two different ranges of periods (or two depth intervals) and in two different ways, the Zstrike and the Tipper strike. The Zstrike always has 90° ambiguity, while the Tipper strike which is based on the z component of the magnetic field (H_z) does not include this ambiguity. The z component was only measured in relatively few soundings and that is the reason why the Tipper doesn't appear for some of the MT soundings.

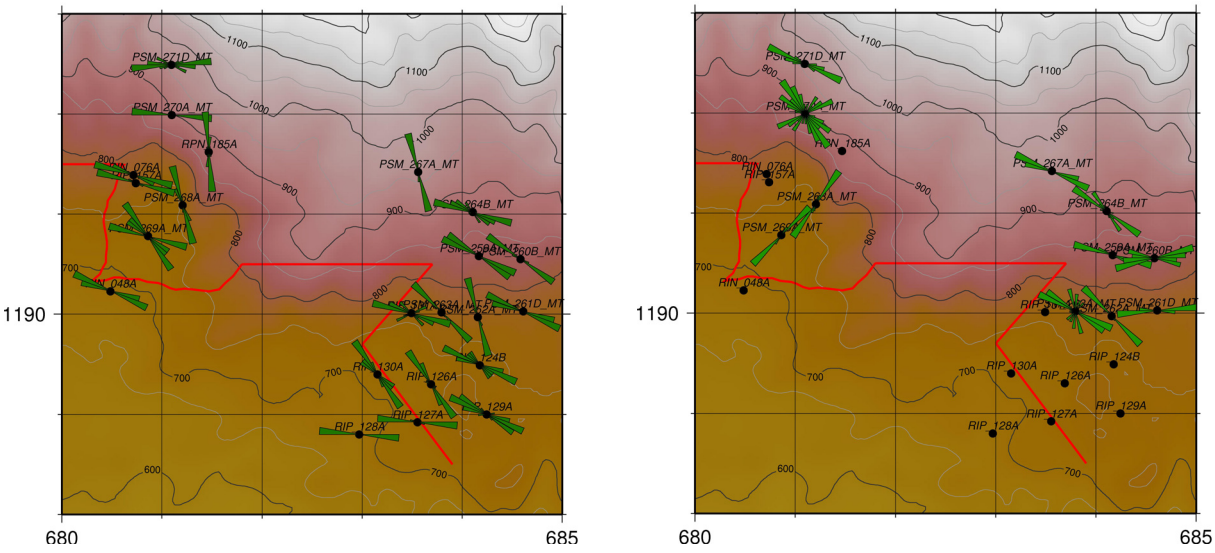

FIGURE 23: Rose diagram of the electrical strike based on Zstrike (a), and Tipper strike (b) for the period from 0.01 to 1 s. Black dots denote MT soundings, while red line marks the national park

In Figure 23, the Zstrike and Tipper strike for frequencies between 1 and 100 Hz are shown, reflecting structures down to a depth of around 2-4 km. We can see how most of the soundings have a trend of -45° (azimuth) for both the Zstrike and Tipper, which agrees with the geological strike of the area. There are two soundings where the Tipper strike is approximately 45° (-135°). They could be suggesting a structure in that direction, because they are very clearly oriented.

In Figure 24, we have the Zstrike and the Tipper strike for frequencies between 1 and 0.001 Hz, representing greater depths (greater than 2-4 km). The Zstrike has the same value as for high frequencies because we constrained the ambiguity according to the geological strike. The non-ambiguous Tipper strike changes especially in the western part of the survey area. It seems that there is a structure suggested by the -45° value, which is different from the one in the eastern part of the area. In the Santa María zone, the Tipper changes from -45° to -90° at shallow and deeper depths,

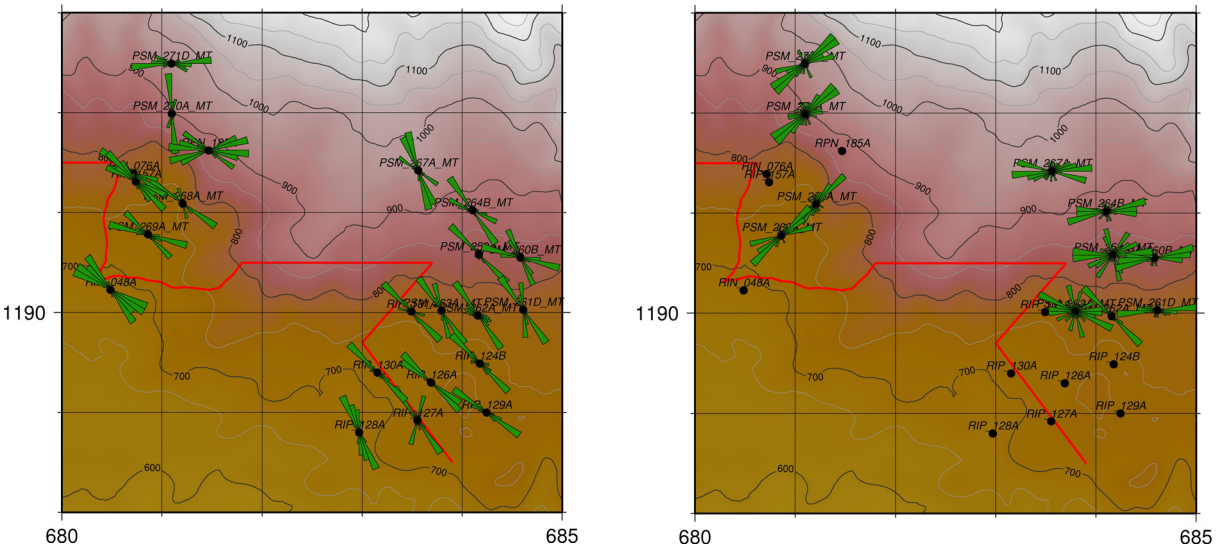

FIGURE 24: Rose diagram of the electrical strike based on Zstrike (a), and Tipper strike (b), for the period from 1 to 1000 s. Black dots denote MT soundings, while red line marks the national park

respectively. It is important to note that the Tipper strike for shallow depths (above 2-4 km) suggests a structural intersection around sounding RPN_185A, which is located close to the possible heat source according to the resistivity model; this could be acting as a pathway for fluid flow. In the same zone the Tipper at greater depths suggests the presence of a deep structure running northeast-southwest (-135°). This deep structure could be a fracture through which fluids flow to the surface (up flow zone), represented by geothermal manifestations in the zone as shown in Figure 22.

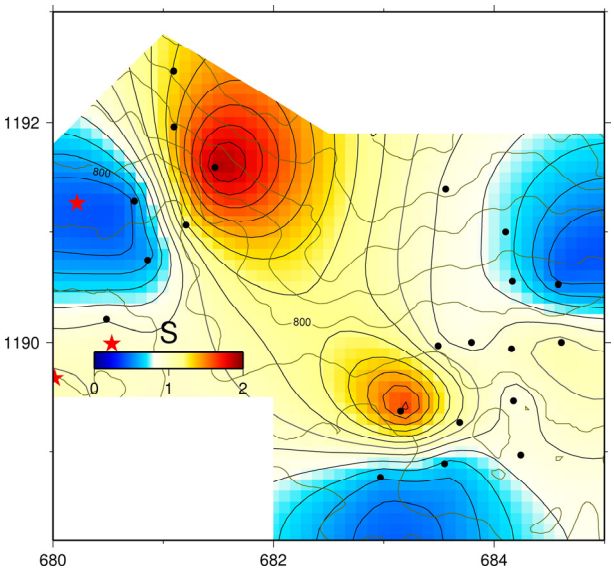

FIGURE 25: Static shift map. Black dots denote MT soundings and red stars denote deep wells (well 3 is shown in the northern part and well 2 in the southeast part)

7.2 Static shift

Figure 25 shows the static shift map of the area where we can see there are parts of the area which can bring distortion effects to the results if the static shift was not corrected for. A shift down by S = 0.1 will result in 10 times too low resistivity values and about three times too small depths to resistivity boundaries (Árnason, 2008). In this map we can only trust the values where the soundings are located, but not in the zone between the two study areas because those values are only an interpolation effect.

Figure 26 shows the histogram of the static shift values. There are two soundings for which the static shift value was close to 2, but most of the shift multipliers (70%) are between 0.5 and 1, which means that most of the MT curves were shifted up.

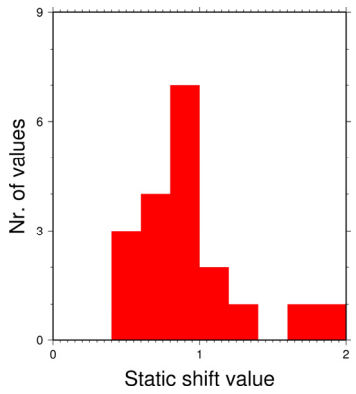

FIGURE 26: Static shift histogram

7.3 Resistivity cross-sections

Figures 27-37 show 7 different resistivity cross-sections in the Las Pailas field, the first four reaching down to a depth of 5,000 and 10,000 m b.s.l., respectively. The results of the cross-sections are discussed in Section 7.5.

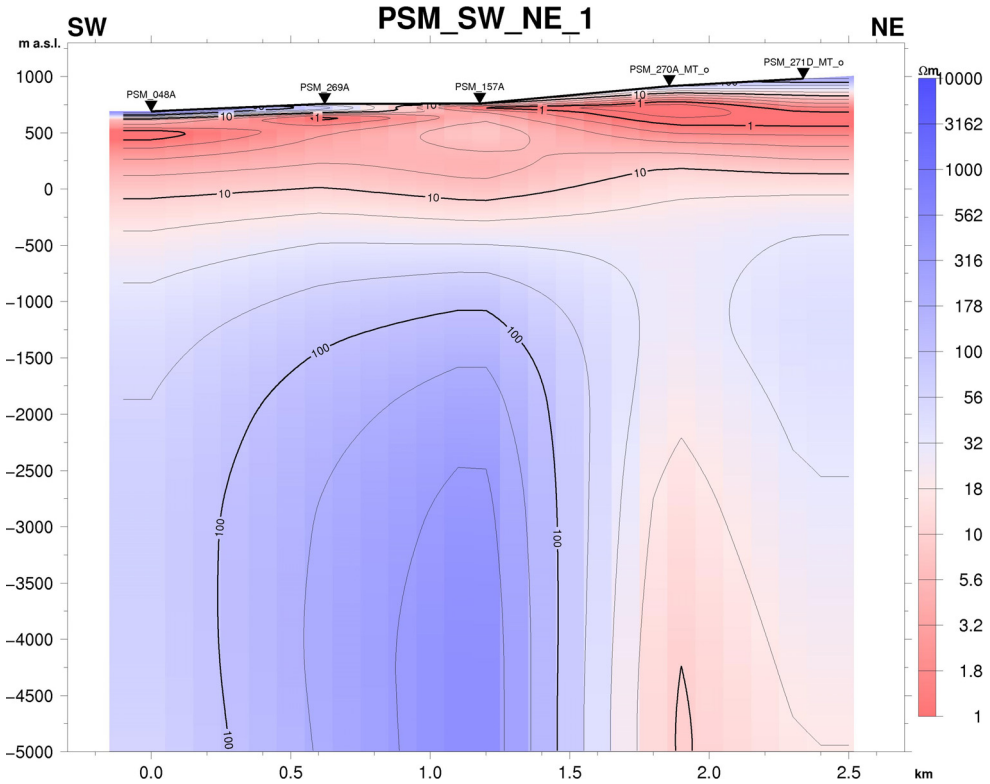

FIGURE 27: Resistivity cross-section PSM_SW_NE_01 down to 5000 m b.s.l.; for location, see Figure 22

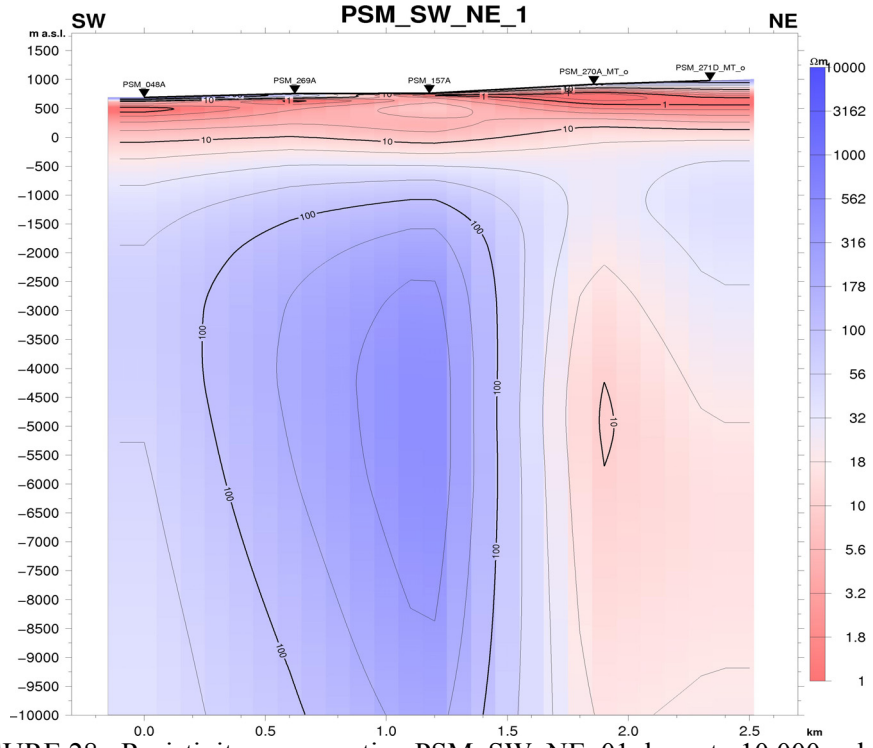

FIGURE 28: Resistivity cross-section PSM_SW_NE_01 down to 10,000 m b.s.l.; for location, see Figure 22

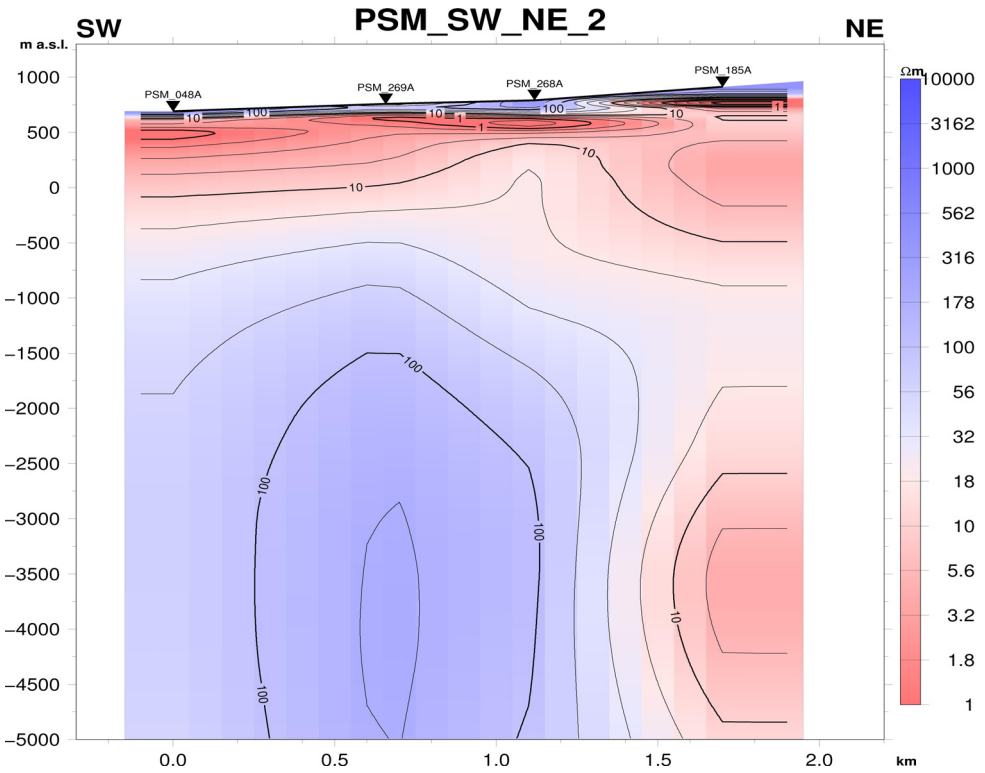

FIGURE 29: Resistivity cross-section PSM_SW_NE_02 down to 5000 m b.s.l.; for location, see Figure 22

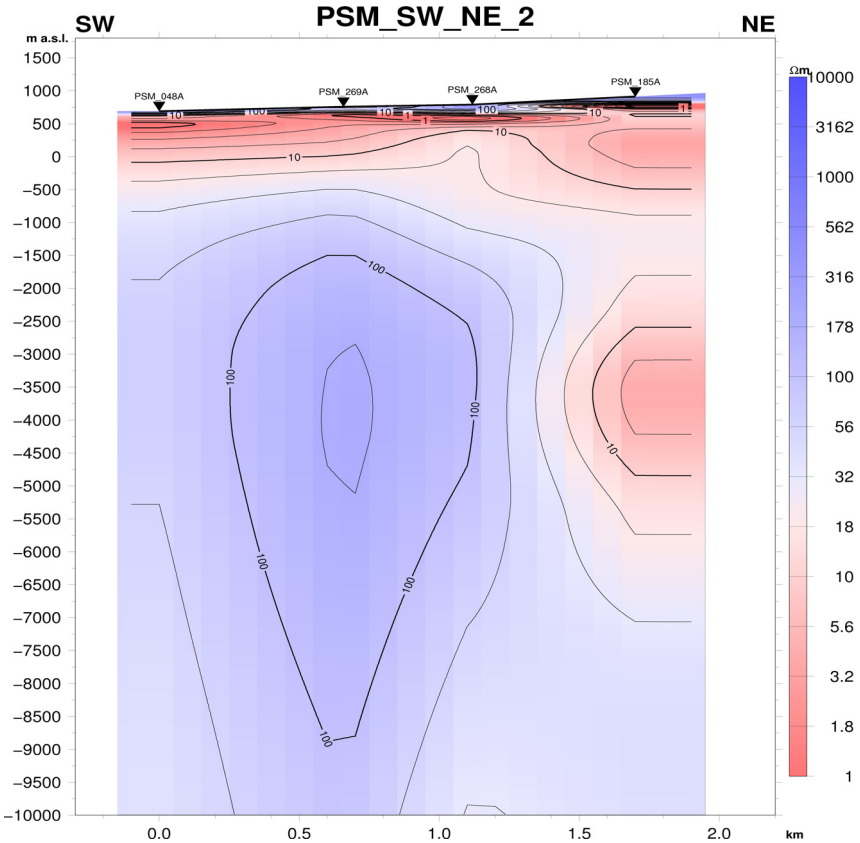

FIGURE 30: Resistivity cross-section PSM_SW_NE_02 down to 10,000 m b.s.l.; for location, see Figure 22

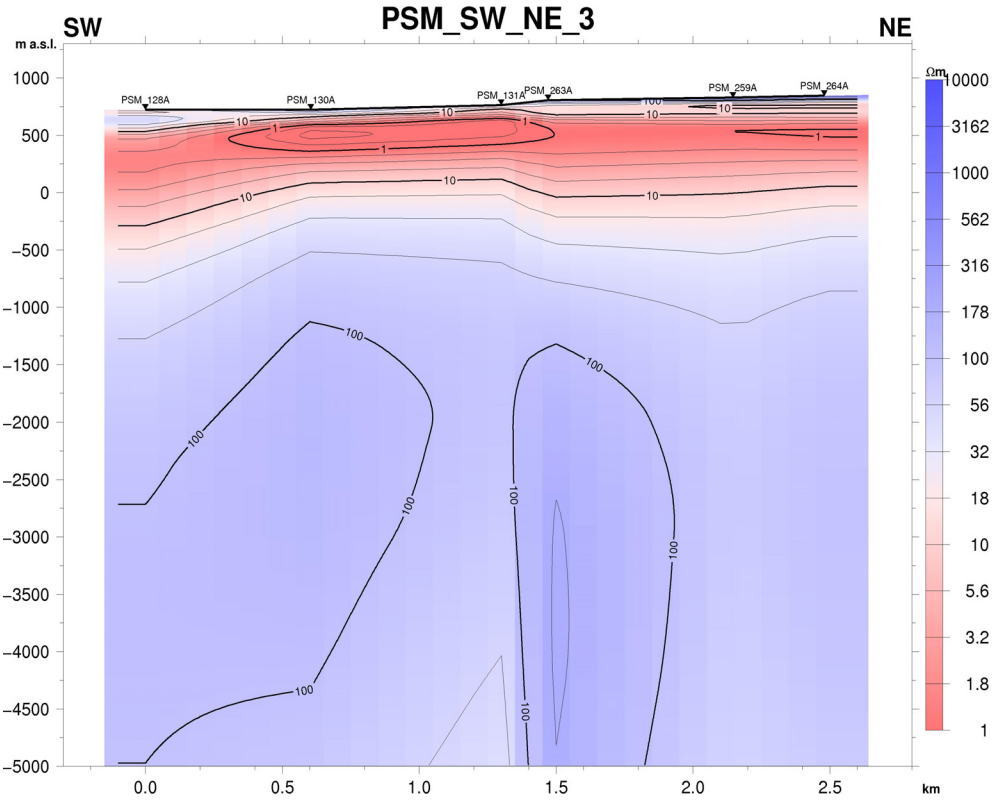

FIGURE 31: Resistivity cross-section PSM_SW_NE_03 down to 5000 m b.s.l.; for location, see Figure 22

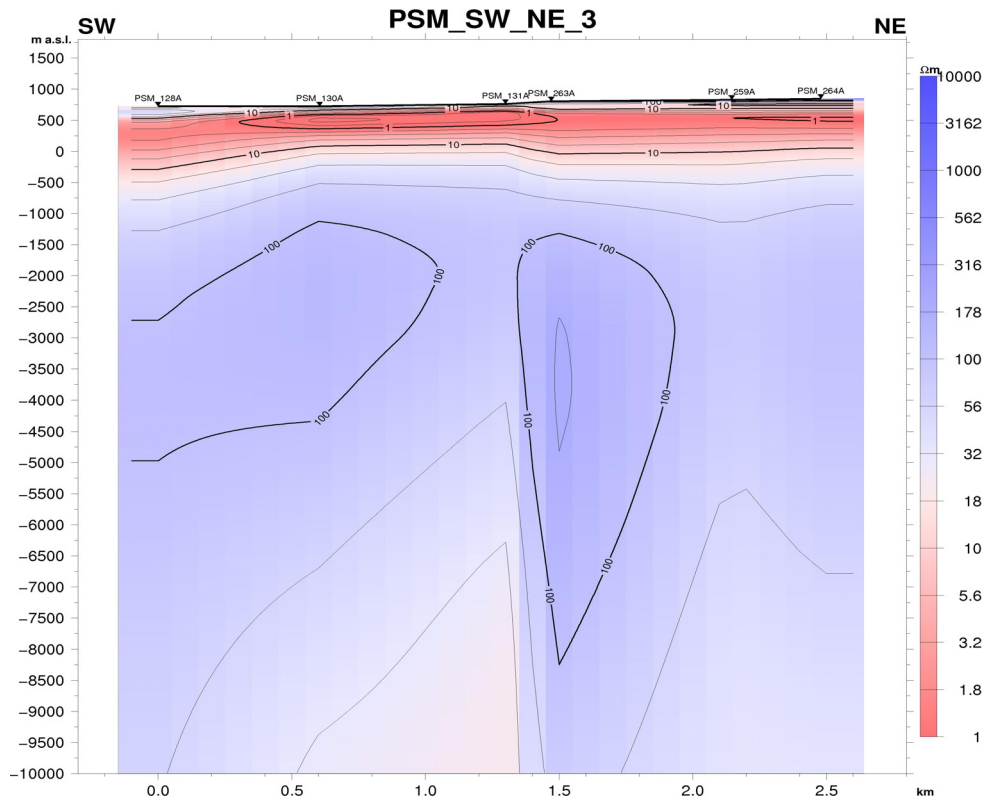

FIGURE 32: Resistivity cross-section PSM_SW_NE_03 down to 10,000 m b.s.l.; for location, see Figure 22

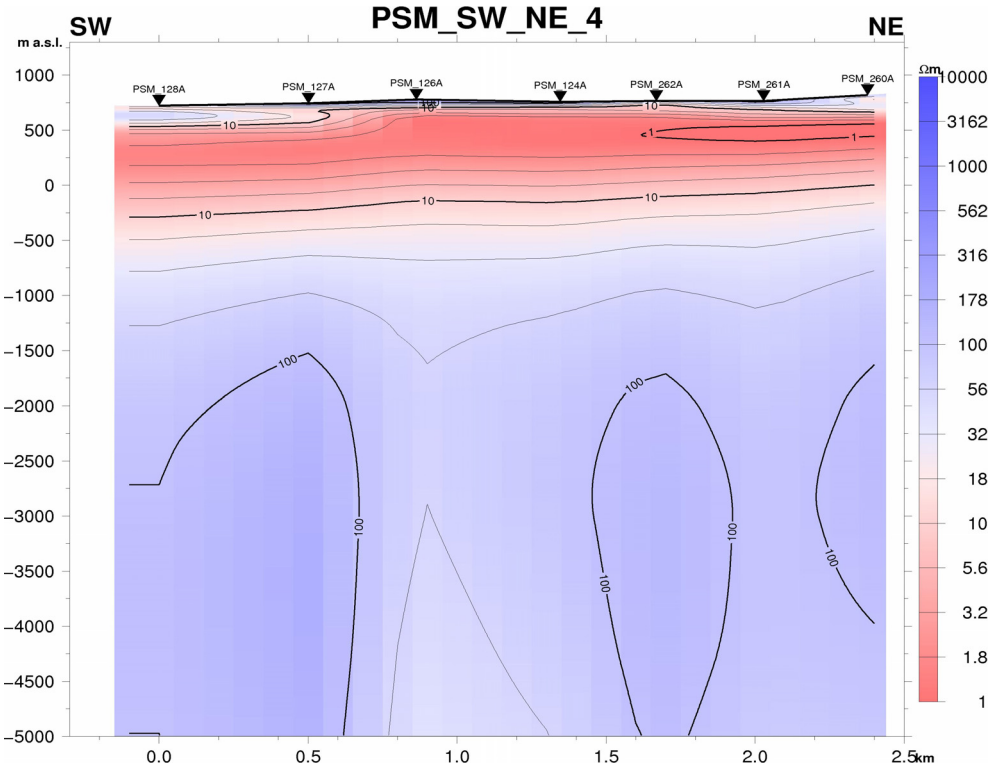

FIGURE 33: Resistivity cross-section PSM_SW_NE_04 down to 5000 m b.s.l.; for location, see Figure 22

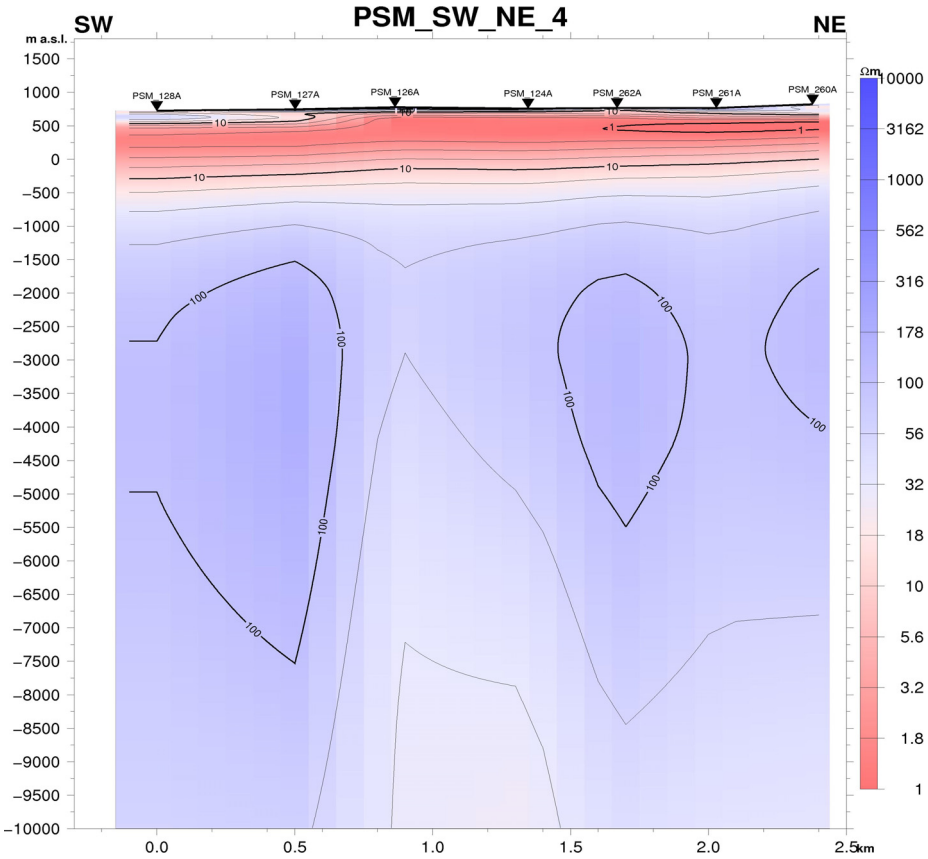

FIGURE 34: Resistivity cross-section PSM_SW_NE_04 down to 10,000 m b.s.l.; for location, see Figure 22

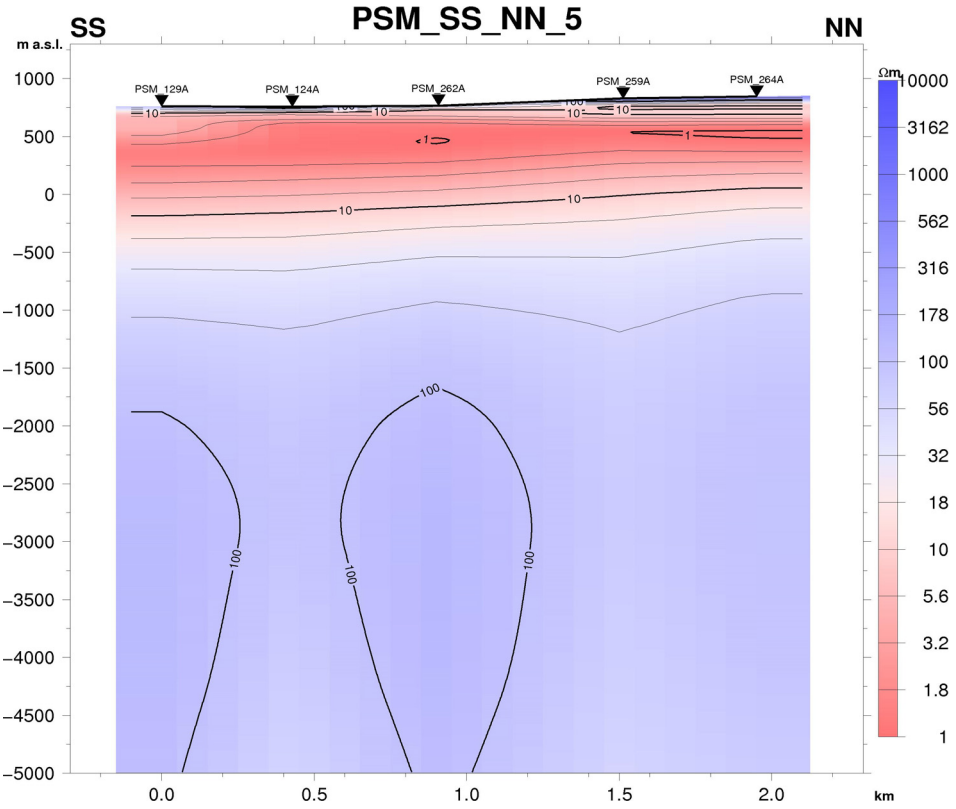

FIGURE 35: Resistivity cross-section PSM_SS_NN_05 down to 5000 m b.s.l., for location, see Figure 22

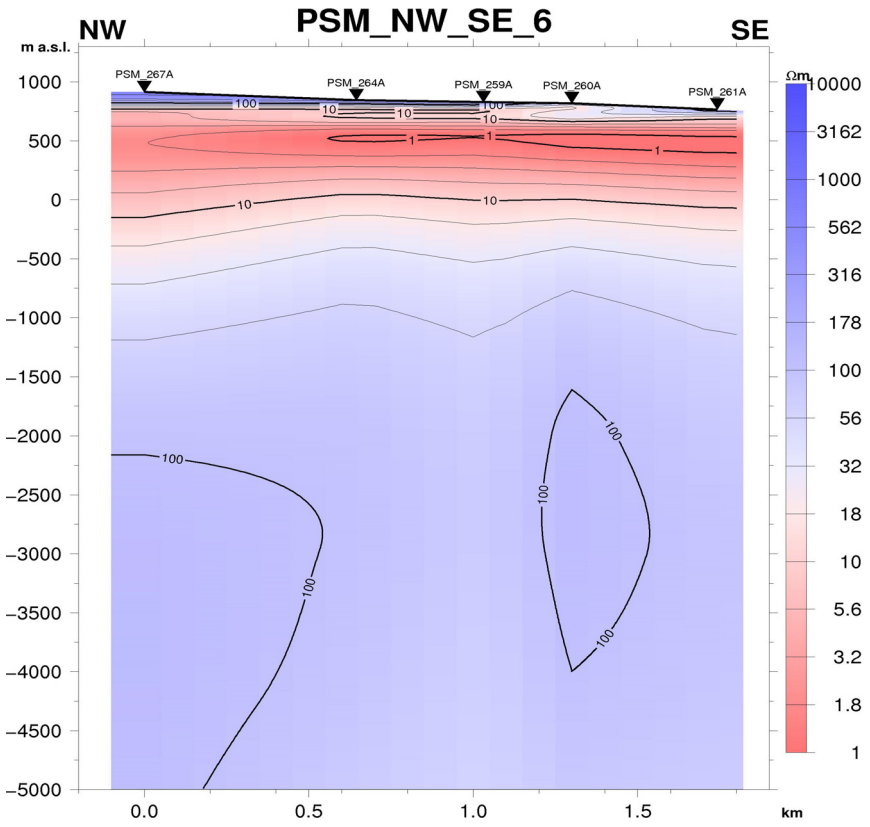

FIGURE 36: Resistivity cross-section PSM_NW_SE_06 down to 5000 m b.s.l., for location, see Figure 22

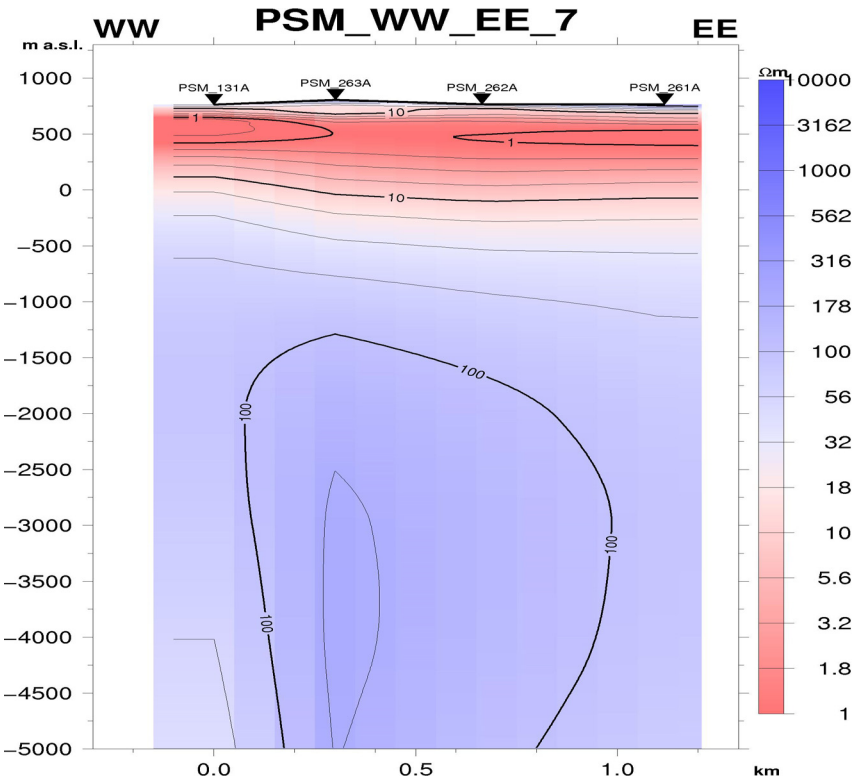

FIGURE 37: Resistivity cross-section PSM_WW_EE_07 down to 5000 m b.s.l., for location, see Figure 22

7.4 Iso-resistivity maps

Figures 38-41 show 4 different iso-resistivity maps of the Las Pailas field, at 500 m a.s.l. and at 1000, 3000 and 5000 m b.s.l., respectively. Results of the iso-resistivity maps are discussed in Section 7.5.

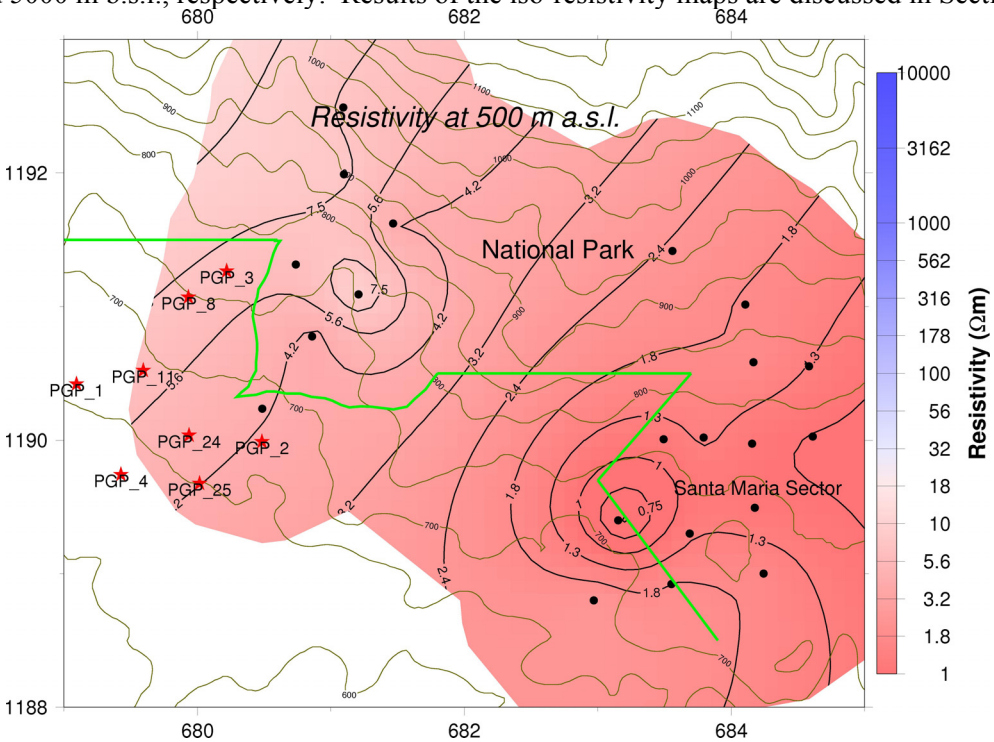

FIGURE 38: Resistivity map at 500 m a.s.l.; black dots denote MT soundings, red stars denote wells and green line marks the national park

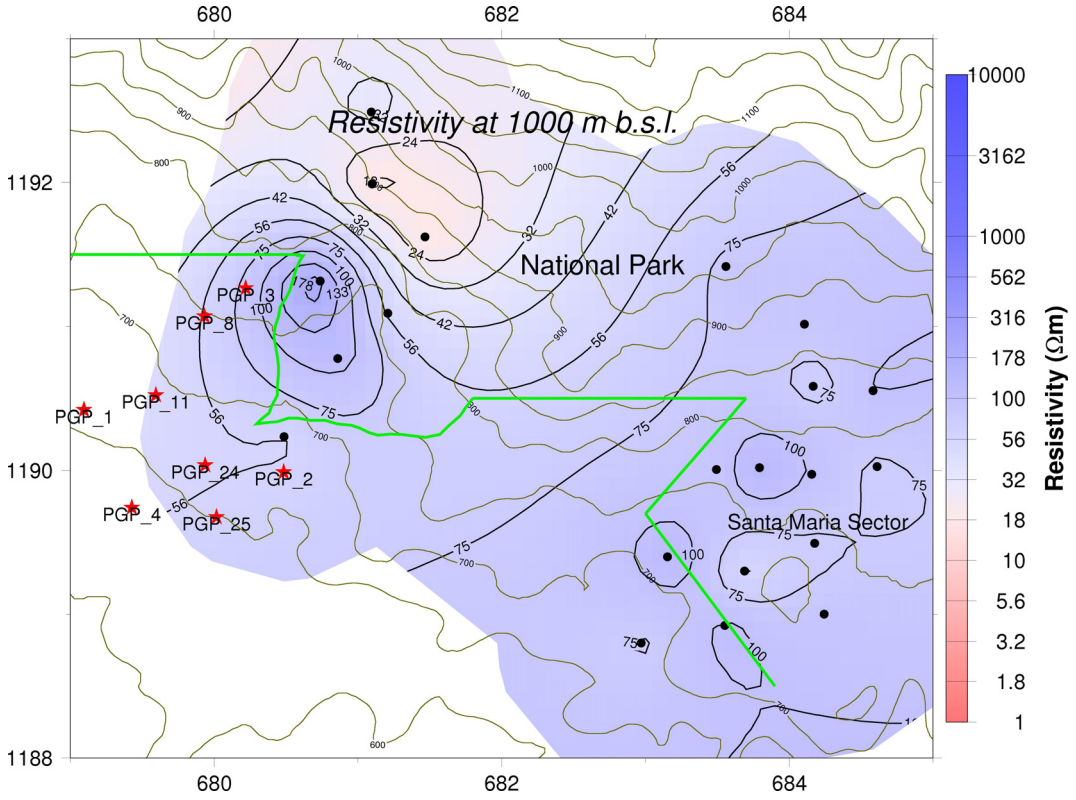

FIGURE 39: Resistivity map at 1000 m b.s.l.; black dots denote MT soundings, red stars denote wells and green line marks the national park

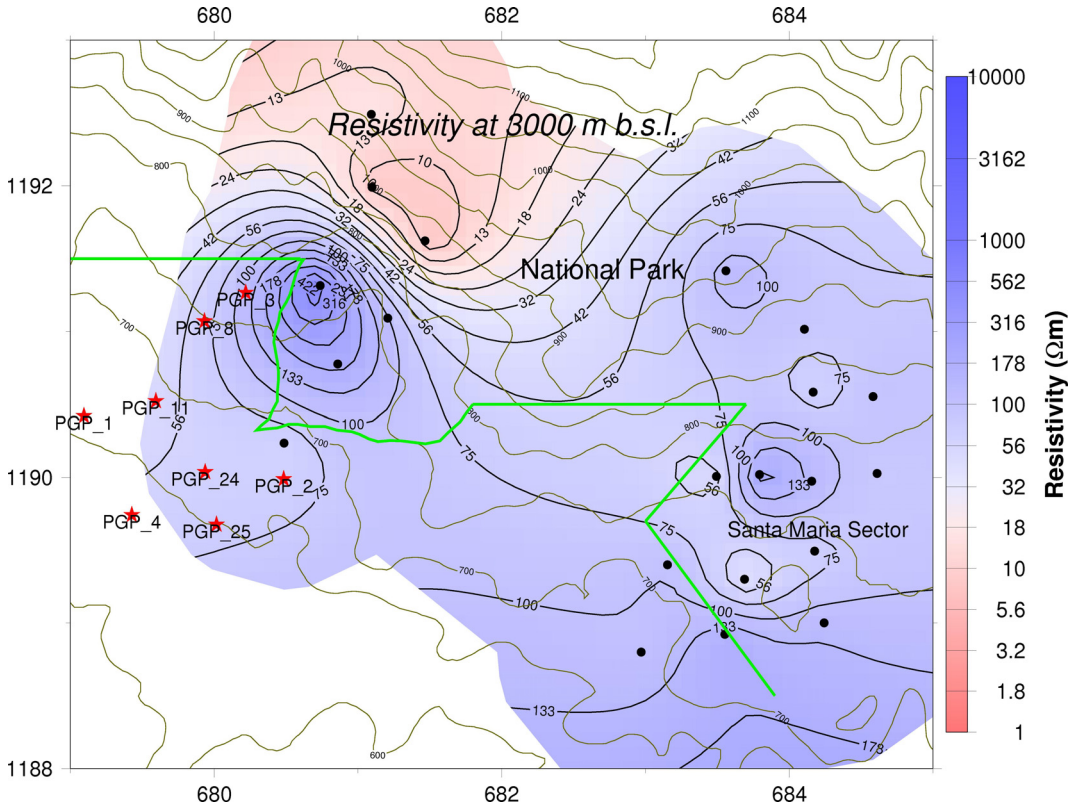

FIGURE 40: Resistivity map at 3000 m b.s.l.; black dots denote MT soundings, red stars denote wells and green line marks the national park

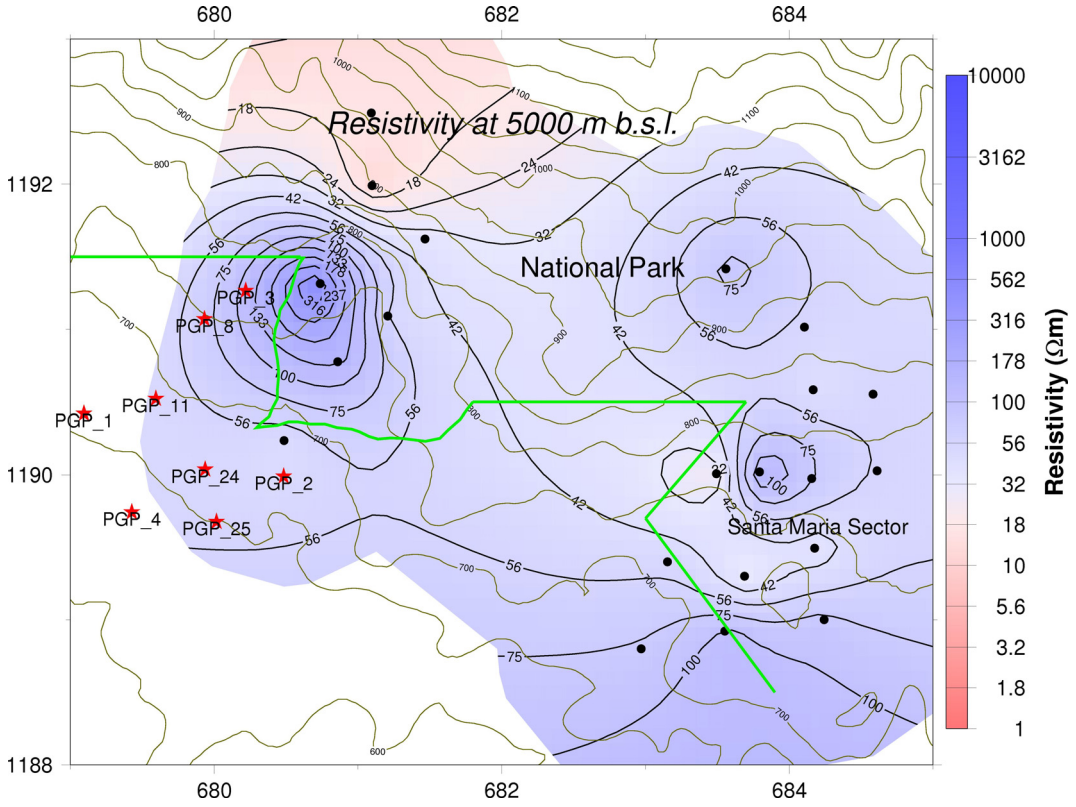

FIGURE 41: Resistivity map at 5000 m b.s.l.; black dots denote MT soundings, red stars denote wells and green line marks the national park

7.5 Interpretation in terms of geothermal signatures

The resistivity cross-sections from 1D joint inversion of MT and TEM data show three major resistivity structures which can be correlated with the model shown in Figure 42; the uppermost high-resistivity layer has resistivity values higher than 10 Ωm. Below there is a conductive cap with values lower than 10 Ωm underlain by a high-resistivity core with resistivity values higher than 100 Ωm. Between these two last layers, there are always intermediate resistivities seen in all of the cross-sections.

In the resistivity cross-section of profile 1, shown in Figure 27, it is possible to see in the shallow part high resistivities (ρ > 50 Ωm), associated with unaltered rocks. Next there is a well-defined low resistivity cap (ρ from 1 to 10 Ωm) which is interpreted as smectite-zeolite clays, related

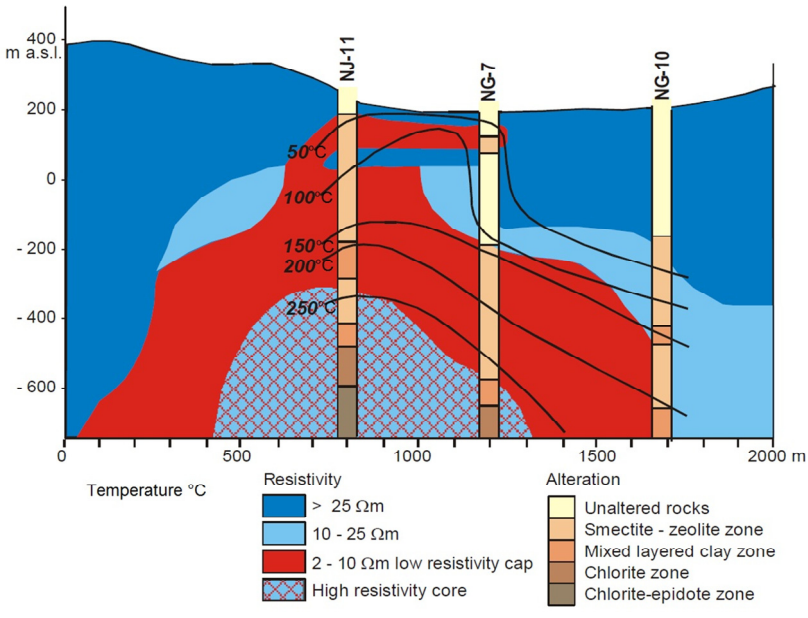

FIGURE 42: Resistivity cross-section from Nesjavellir geothermal field, SW-Iceland, alteration zoning and temperature (modified from Árnason et al., 1987)

to temperatures between 100 and 230°C, like in Figure 42. It is possible to see low resistivity in the very shallow part, i.e. around sounding RIP_157A (PSM_157A), which is well correlated with geothermal manifestations in the area, as seen in Figures 20, 21 and 22. Below 1000 m b.s.l., a high-resistivity body appears (resistivity higher than 100 Ωm) beneath soundings PSM_269A and RIP_157A (PSM_157A); this might be interpreted as the high-resistivity core, where alteration minerals such as chlorite and epidote would be present. In Figure 28, it is clearly seen that below soundings PSM_270A and PSM_271D, a low-resistivity body appears at 2000 and 4000 m b.s.l., respectively, which may be associated with a possible heat source.

Figures 29 and 30 show resistivity cross-sections of profile 2 down to depths of 5000 and 10,000 m b.s.l., respectively. It is possible to see a resistivity structure similar to the one seen in profile 1. The main anomalies in this cross-section are the high-resistivity core appearing at 1000 m b.s.l. which is correlated with the chlorite and epidote clays as in profile 1; and the deep conductor below sounding PSM_185A (RPN_185A) beneath 2000 m b.s.l., which is well correlated with the conductor seen in profile 1, representing what may be interpreted as a possible heat source.

In Figures 31 and 32 we have the resistivity cross-sections for profile 3 down to depths of 5000 and 10,000 m b.s.l., respectively. In these sections we can see a resistivity structure similar to the ones in profiles 1 and 2, showing in the shallow part high resistivities (unaltered rocks), then a very low resistivity, the low-resistivity cap associated with the smectite-zeolite clays and below 1000 m b.s.l. a high-resistivity core interpreted as the chlorite-epidote zone with temperatures higher than 230°C. In Figure 32, it is possible to see below approximately 6000 m b.s.l. and between soundings PSM_130A (RIP_130A) and PSM_131A (RIP_131A), an indication of a deep lying conductor, which may be related to a possible heat source in the zone.

The resistivity cross-section of profile 4 is shown in Figures 33 and 34, down to depths of 5000 and 10,000 m b.s.l., respectively. The resistivity structure for this section is very similar to profile 3 because we have the high-low-high model again and the three zones are still well defined. In Figure 34, the deep conductor can be seen appearing again below 7000 m b.s.l., which is well correlated with profile 3 and with a possible heat source, but this could also be a suggestion of the continuity of structure NF7, shown in Figure 20, in that zone.

For the cross-sections shown in Figures 35, 36 and 37, related to profiles 5, 6 and 7, it is possible to identify a resistivity structure very similar to that described above for profiles 3 and 4, and that means that they are well correlated at least down to 5000 m b.s.l., but here it is not possible to see a deep conductor as in profiles 3 and 4.

In Figure 38, the resistivity map at 500 m a.s.l. shows the distribution of a probable smectite-zeolite clay cap, because a well-defined conductor is seen at approximately this elevation with resistivity values characteristic for these alteration minerals which are found at temperatures between 100 and 230°C.

Resistivities higher than 50 Ωm are seen in the major part of the map in Figure 39, displaying resistivity at 1000 m b.s.l., what could be interpreted as part of the high-resistivity core, and associated with alteration minerals like chlorite and epidote with temperatures higher than 230°C. Here we see lower resistivity in two soundings.

The resistivity map at 3000 m b.s.l. is shown in Figure 40 and the most important fact that can be seen there is the low-resistivity body (deep conductor) to the northern part of the study area, which could be interpreted as a possible heat source; it is still apparent at 5000 m b.s.l., as can be seen in Figure 41. This is well correlated with the actual conceptual model of the area, suggesting the location of the heat source in that zone. Note also an indication of low resistivity at depth in the Santa María Sector for these last two resistivity maps.

Here it should though be emphasized what was explained in Section 2.2.4, that "resistivity reflects alteration mineralogy but not necessarily the temperature" (Árnason et al., 2000). If the alteration and temperature are in equilibrium, the resistivity structure reflects not only the alteration but also temperature. In most cases, the resistivity can be regarded as a "maximum thermometer". It means that if the temperature that produced the alteration mineralogy prevails, the resistivity structure can be used to predict the temperature but, if cooling has occurred, the alteration remains and so does the resistivity structure. The deep seated low-resistivity body indicates a possible heat source at depth and hence upflow of heat driving the geothermal system.

8. CONCLUSIONS AND RECOMMENDATIONS

- A well-defined low-resistivity conductor was detected at around 400 m depth in all of the resistivity cross-sections from the 1D joint inversion of MT and TEM data, and is also seen in the resistivity map at 500 m a.s.l.; this is presumably associated with a smectite and zeolite clay cap. The low-resistivity cap and the adjacent mixed-layered clay zone are underlain by a high-resistivity core, which represents a zone where chlorite and epidote are the dominant alteration minerals. Provided there is equilibrium between alteration and the present temperature, the high-resistivity core indicates temperatures exceeding 230°C.

- In the northern part of the Las Pailas sector, the resistivity maps show a deep lying conductor which could be associated with a deep seated heat source. A similar conductor was also detected at depth in the Santa María sector for profiles 3 and 4, which could be related to a heat source and with the existence of structure NF7 in that zone.

- Joint 1D inversion of MT and TDEM data solves the static shift problem of MT soundings, giving a more reliable model from the data.

- The Tipper strike distribution for the period ranging from 0.01 to 1 s, shown in Figure 23, and specifically for soundings PSM_270A and PSM_271D, agrees not only with the geological strike (running NW-SE) but also with important changes in resistivity (SW-NE) around sounding RPN_185A (PSM_185A), which are believed to be associated with the suggested structure NF7, running NW-SE.

- The Tipper strike distribution (running SW-NE) shown in Figure 24 for the period ranging from 1 to 1000 s, especially for soundings PSM_268A, PSM_269A, PSM_270A and PSM_271D, can be, with resistivity maps at 1000 and 3000 m b.s.l., interpreted as a possible intersection of fractures acting as a pathway for fluid flow.

- The main recommendation is to collect more MT and TDEM data to create some profiles for filling the space between the two areas studied in this work. It is also recommended to add more soundings in the northern part of Las Pailas geothermal field, to better delineate the geothermal reservoir and give better constraints on the deep seated heat source.

ACKNOWLEDGEMENTS

I wish to express my gratitude to the United Nations University Geothermal Training Programme and the Government of Iceland for giving me the possibility to participate in this specialized training. I am also very thankful to the Orkustofnun and ÍSOR staff members for their good lectures and assistance in all respects.

I would like to express my gratitude to the director of the UNU-GTP, Dr. Ingvar B. Fridleifsson, and the deputy director, Mr. Lúdvík S. Georgsson, for nominating me to participate in the training. I am grateful to the UNU-GTP staff, Ms. Thórhildur Ísberg, Mr. Markús A.G. Wilde and Mr. Ingimar G. Haraldsson for their continuous help during my stay in Iceland.

Special thanks to my advisors, Mr. Gylfi Páll Hersir and Mr. Knútur Árnason, for their invaluable help from the beginning to end. I want to thank them for their guidance, for all their patience, countless hours spent explaining and discussing various problems, and for giving helpful comments. Many thanks go to Mrs. Ragna Karlsdóttir for giving helpful comments and recommendations.

Many thanks go to all the other UNU Fellows for valuable discussions on various disciplines of geothermal exploration and for their friendship.

I would like to express my great gratitude to ICE – the Instituto Costarricense de Electricidad for allowing me to participate in this training programme.

Finally, I want to thank the almighty God, because he gave me the opportunity and the fortitude to complete this stage of my life successfully.

REFERENCES

Archie, G.E., 1942: The electrical resistivity log as an aid in determining some reservoir characteristics. *Tran. AIME, 146,* 54-67.

Arias, M., 2002*: Tecto-caldera Cañas Dulces-Guachipelin, Costa Rica*. Instituto Costarricense de Electricidad, internal report (in Spanish), 19 pp.

Árnason, K., 1989: *Central-loop transient electromagnetic sounding over a horizontally layered earth*. Orkustofnun, Reykjavík, report OS-89032/JHD-06, 129 pp.

Árnason, K., 2006a: *TemX. A graphically interactive program for processing central-loop TEM data, a short manual.* ÍSOR – Iceland GeoSurvey, Reykjavík, 10 pp.

Árnason, K., 2006b: *TEMTD. A program for 1D inversion of central-loop TEM and MT data, a short manual.* ÍSOR – Iceland GeoSurvey, Reykjavík, 16 pp.

Árnason, K., 2008: *The magneto-telluric static shift problem*. ÍSOR – Iceland GeoSurvey, Reykjavík, report ISOR-08088, 17 pp.

Árnason, K., Eysteinsson, H., and Hersir, G.P., 2010: Joint 1D inversion of TEM and MT data and 3D inversion of MT data in the Hengill area, SW Iceland. *Geothermics, 39,* 13-34.

Árnason, K., Karlsdóttir, R., Eysteinsson, H., Flóvenz, Ó.G., and Gudlaugsson, S.Th., 2000: The resistivity structure of high-temperature geothermal systems in Iceland. *Proceedings of the World Geothermal Congress 2000, Kyushu-Tohoku, Japan,* 923-928.

Árnason, K., Haraldsson, G.I., Johnsen, G.V., Thorbergsson, G., Hersir, G.P., Saemundsson, K., Georgsson, L.S., Rögnvaldsson, S.Th., and Snorrason, S.P., 1987: *Nesjavellir-Ölkelduháls, surface exploration 1986.* Orkustofnun, Reykjavík, report OS-87018/JHD-02 (in Icelandic), 112 pp + maps.

Badilla, D., 2011: *Appendices to the report "Resistivity imaging of the Santa Maria sector and the northern zone of Las Pailas geothermal area, Costa Rica, using joint 1D inversion of TDEM and MT data"*. UTP-GTP, Iceland, report 8, appendices, 49 pp.

Barrantes, M., 2006: Geo-environmental aspects for the development of Las Pailas geothermal field, Guanacaste, Costa Rica. Report 8 in: *Geothermal Training in Iceland 2006*. UNU-GTP, Iceland, 121-151.

Cagniard, L., 1953: Basic theory of the magneto-telluric method of geophysical prospecting. *Geophysics, 18,* 605-635.

Castro, S., 2002: Reservoir engineering studies in the Las Pailas geothermal field, Costa Rica. Report 4 in: *Geothermal Training in Iceland 2002.* UNU-GTP, Iceland, 1-26.

Chavarría, L., Mora, O., Hakanson, E., Galvez, M., Rojas, M., Molina, F., and Murillo, A., 2010: Geologic model of the Pailas geothermal field, Guanacaste, Costa Rica. *Proceedings of the World Geothermal Congress 2010, Bali, Indonesia*, 4 pp.

Chavarría, L., Mora, O., Hakanson, E., Molina, F., Vega, E., Torres, Y., Vallejos, O., Yock, A., Lezama, G., and Castro S., 2006: *Development strategies for Las Pailas geothermal field (in Spanish)*. Consultors Panel, Instituto Costarricense de Electricidad, Guanacaste, Costa Rica, 40 pp.

Dakhnov, V.N., 1962: Geophysical well logging. Q. *Colorado Sch. Mines*, 57-2, 445 pp.

Deer, W.A., Howie, R.A., and Zussman, J., 1962: *Rock-forming minerals, vol. 3: Sheet silicates*. Longmans, Green and Co. Ltd., London, 270 pp.

DeMets, C. 2001: A new estimate for present-day Cocos-Caribbean plate motion: Implications for slip along the Central American volcanic arc. *Geophys. Res. Letters, 28,* 4043-4046.

DeMets, C., Gordon, R.G., Argus, D.F., and Stein, S., 1990: Current plate motions. *Geophys. J. Int., 101*, 425-478.

Flóvenz, Ó.G., Spangenberg, E., Kulenkampff, J., Árnason, K., Karlsdóttir, R., and Huenges E., 2005: The role of electrical conduction in geothermal exploration. *Proceedings of the World Geothermal Congress 2005, Antalya, Turkey*, CD, 9 pp.

GeothermEx Inc., 2001: *Pre-feasibility studies of the Las Pailas geothermal project, Costa Rica*. Instituto Costarricense de Electricidad, report, San José.

Hersir, G.P., and Árnason, K., 2009: Resistivity of rocks. *Paper presented at the "Short Course on Surface Exploration for Geothermal Resources", organized by UNU-GTP and LaGeo, Santa Tecla, El Salvador*, 8 pp.

Hersir, G.P., and Björnsson, A., 1991: *Geophysical exploration for geothermal resources. Principles and applications.* UNU-GTP, Iceland, report 15, 94 pp.

Keller, G.V., and Frischknecht, F.C., 1966: *Electrical methods in geophysical prospecting.* Pergamon Press Ltd., Oxford, 527 pp.

Kempter, K.A., 1997: *Geologic evolution of the Rincón de la Vieja volcano complex, northwestern Costa Rica.* University of Texas, PhD thesis, 159 pp.

Kempter, K.A., Benner, S.G., and Williams, S.N., 1996: The Rincón de la Vieja volcano, Guanacaste

province, Costa Rica: Geology of the southwestern flank and hazards implications. *J. Volcanol. & Geotherm. Res., 71,* 109-127.

Lee Lerner, K., Lerner, B.W., and Cengage, G., 2003: *Porosity and permeability.* World of Earth Science, webpage: *www.enotes.com/earth-science/*

Molina, F., 2000: Las Pailas geothermal area, Rincón de la Vieja volcano, Costa Rica. Report 13 in: *Geothermal Training in Iceland 2000.* UNU-GTP, Iceland, 267-284.

Phoenix Geophysics, 2009: *Data processing. User's guide*. Phoenix Geophysics, Ltd., Toronto.

Pytte, A.M., and R.C., Reynolds, 1989: The thermal transformation of smectite to illite. In: Naeser, N.D., and McCulloh, T.H. (eds.), *Thermal history of sedimentary basins*. Springer-Verlag, NY, 51-64.

Quist, A.S., and Marshall, W.L., 1968: Electrical conductances of aqueous sodium chloride solutions from 0 to 800°C and at pressures to 4000 bars. *J. Phys. Chem*., 72, 684-703.

Rowland, B.F., 2002: *Time-domain electromagnetic exploration.* Northwest Geophysical Associates, Inc., 6 pp.

Simpson, F., and Bahr, K., 2005: *Practical magnetotellurics*. Cambridge University Press, Cambridge, UK, 270 pp.

Sternberg, K.B., Wasburne, J.C., and Pellerin, L., 1988: Correction for the static shift in magnetotellurics using transient electromagnetic soundings. *Geophysics, 53-11,* 1459-1468.

Tikhonov, A.N., 1950: The determination of electrical properties of the deep layers of the earth's crust. Dokl. *Acad. Nauk., SSR 73,* 295-297 (in Russian).

Tucker, M.E., 1991: *Sedimentary petrology* (2nd ed.). Blackwell Scientific Publ., London, 260 pp.

Ward, S.H, and Wannamaker, P.E., 1983: *The MT/AMT electromagnetic method in geothermal exploration*. UNU-GTP, Iceland, report 5, 107 pp.